PHILOSOPHICAL TRANSACTIONS OF THE ROYAL SOCIETY A MATHEMATICAL, PHYSICAL & ENGINEERING SCIENCES

A Coherent Structure Model of the Turbulent Boundary Layer and Its Ability to Predict Reynolds Number Dependence

R. E. Falco

Phil. Trans. R. Soc. Lond. A 1991 **336**, 103-129
doi: 10.1098/rsta.1991.0069

A coherent structure model of the turbulent boundary layer and its ability to predict Reynolds number dependence

By R. E. Falco

Turbulence Structure Laboratory, Department of Mechanical Engineering, Michigan State University, East Lansing, Michigan 48824, U.S.A.

The coherent motions identified in passively marked turbulent boundary-layer experiments are reviewed. Data obtained in our laboratory using simultaneous hot-wire anemometry and flow visualization are analysed to provide measures of the percent contribution of the coherent motions to the total Reynolds stress. A coherent structure model is then developed. In the outer region the model incorporates the large-scale motions, the typical eddies and their interactions. In the wall region the model is characterized by the long streaks, their associated hairpin vortices, and the pockets with their associated pocket and hairpin vortices. The motions in both regions have unique phase relations which play an important role in their evolution and the resulting intensity of their interactions. In addition, the inner–outer region interactions are seen to be strong because typical eddies, microscale motions which can directly initiate the bursting process near a wall, are convected towards the wall by the response of the high speed outer region fluid to the presence of the large-scale motions. This interaction establishes a phasing between the inner and outer regions. The length and velocity scales of the typical eddy are used to remove the Reynolds number dependence of the streamwise fluctuations and the Reynolds stress in the fully turbulent portion of turbulent boundary layers over a wide range of Reynolds numbers.

1. Introduction

The coherent structure of the turbulent boundary layer has been studied for about three decades. Large-scale motions and sublayer structure were initially the centre of attention. These studies constitute an extensive literature which we do not have space to review. The reviews of Robinson *et al.* (1989), Cantwell (1981), Kline & Falco (1979), Kline (1978), Townsend (1976) and Willmarth (1975) should serve to bring the reader to the point where this paper starts.

Although it has been clear for a long time that the drag coefficient decreases, and the turbulent boundary-layer growth rate slows with increasing Reynolds number, these changes have not been related to the coherent structure. In the outer region, Coles (1956) showed that the law of the wake for the mean velocity is Reynolds number dependent for momentum thickness Reynolds numbers, R_θ, less than 5000. In the near wall region, Kline *et al.* (1967) showed that the average spanwise spacing of the streaky structure, λ, scaled on wall variables, u_τ and ν/u_τ. Smith & Metzler (1983) confirmed that $\lambda^+ = 100$, and extended the results to $R_\theta \approx 5000$. However, this value, two orders of magnitude greater than the local characteristic length scale,

Phil. Trans. R. Soc. Lond. A (1991), **336**, 103–129
Printed in Great Britain

has long been unexplained. Furthermore, the shorter sublayer streaks that are characteristic of the boundaries of the pockets of high Reynolds stress (Falco 1980*a*), have a Reynolds number dependence when scaled on wall variables (as discussed below). In addition, our knowledge of the parameters that govern the period between bursts of high Reynolds stress in the wall region, which would shed light on the mechanism that maintains the turbulence, is unsatisfactory. Inner scaling over a narrow range of commonly obtained laboratory Reynolds numbers is currently preferred (see Luchik & Tiederman 1987), but it appears unlikely to hold at high Reynolds numbers (see, for example, Narasimha & Kailas 1987).

In the past fifteen years it has been acknowledged that microscale motions, which are Reynolds number dependent, play an important part in the dynamics of the overall flow. Structural studies of Lu & Willmarth (1973) and Sabot & Comte-Bellot (1975) in the outer region of boundary layers and pipes, respectively, showed that the regions of high Reynolds stress (detected using a Reynolds stress detection technique) were small with respect to the boundary-layer thickness, δ. Falco (1977) used simultaneous hot-wire anemometry and flow visualization to show that microscale coherent motions, which were observed all across the outer region of the boundary layer (Falco 1974), had the length scales of these regions of high Reynolds stress. By comparison with the conditionally sampled data of Antonia (1972), these microscale motions were seen to be important players in the spectrum of the Reynolds stress producing motions. They were called 'typical eddies' and were observed to be strongest when riding along the upstream boundary of the large-scale motions of $O(\delta)$. Falco (1977) also suggested that the typical eddies significantly influenced the large-scale motions at low Reynolds numbers, resulting in a Reynolds number dependence. Murlis *et al.* (1982) showed that the small-scale intermittency which characterized the boundaries of the large-scale motions did correlate with the typical eddies. They found that the intensity of the large eddies increased with Reynolds number although their length scale was independent of Reynolds number. They concluded that the overall shape and large-scale transport of the boundary layer are governed by the large-scale motions at all Reynolds numbers, although the typical eddies may carry significant Reynolds stress at low Reynolds numbers. Antonia *et al.* (1982) also showed that large scale motions had a Reynolds number dependence up to $R_\theta \approx 3000$. They extrapolated typical eddy data of Falco (1977) to estimate the Reynolds stress contribution and found that it decreased rapidly with Reynolds number. This was not unexpected (see Falco 1977) because of the existence of Coles law of the wake for $R_\theta > 5000$, which is Reynolds number independent.

However, the typical eddies continue to be a persistent feature of the flow as the Reynolds number increased. Falco (1977) proposed a model showing the relation of the large scale and typical eddy motions. This provided an explanation for the time between bursts appearing to have little variation across the layer, although the length scales of these bursts remained small (Lu & Willmarth 1973; Sabot & Comte-Bellot 1976). Furthermore, this phasing suggested the role of these microscale motions in the bursting process at the wall. Falco (1978, 1980*c*, 1982, 1983) found a strong correlation between the typical eddies and the ejections, sweeps, pockets and hairpin vortices found in the wall region. The typical eddies were observed to directly create pockets and some of the hairpins observed near the wall. Falco (1980*a*, *c*) found that the pockets were initially sweeps, and later in their evolution they were ejections. Falco (1978, 1982, 1983, and references below) directly observed pockets being formed by typical eddies moving over the sublayer. Recently, Falco *et al.*

(1990) found that the typical eddies can also create the long streaks in the sublayer of a turbulent boundary layer, often in prelude to the creation of a pocket. Thus it appears that at low and moderate Reynolds numbers both microscale and large-scale coherent motions are important contributors to the Reynolds stress in the turbulent boundary layer. Both have a Reynolds number dependence, with that of the typical eddies apparently continuing at high Reynolds numbers as $R_\theta^{-0.73}$ (Falco 1974, see update below). However, the persistence of the typical eddy at all Reynolds numbers, with a scale that is of the order of the streak spacing, together with its ability to generate streaks and pockets, and its phasing with the large-scale motions, suggests that it may play a continuing role in the production of turbulence as the Reynolds number increases.

The form of these Reynolds number dependent motions in the outer region of the fully developed turbulent boundary layer is the subject of controversy. Falco (1977) suggested that they were vortex ring-like, and thus not attached to the wall. Earlier flow visualization and analysis of Theodorsen (1955) claimed that hierarchies of hairpins were a dominant feature of wall bounded turbulent flows, with smaller hairpins emanating from larger ones. This is reminiscent of the high Reynolds number vortex tube reconnection studies of Melander & Zabuski (1988). Many authors (see the review of Robinson *et al.* 1989) have observed hairpins in the near wall region of fully developed turbulent boundary layers. Head & Bandyopadhyay (1981), using tilted light sheet flow visualization, argued that the typical eddies seen in the outer part of the layer extended across it and were attached to the wall, and thus were extended hairpins. Falco (1980*a*) used mutually orthogonal laser sheets to determine uniquely whether the typical eddies found in the outer intermittent part of the turbulent boundary layer were hairpins or rings. One light sheet was perpendicular to the wall and parallel to the stream, and the other parallel to the wall. When the top of a typical eddy was observed in the streamwise-normal light sheet, he searched for evidence of its 'legs' passing through the sheet parallel to the wall. Results showed that the typical eddies were spatially compact structures (when viewed on the scale of δ), and are better described as rings than hairpins.

It has been difficult to incorporate coherent structure information into a model for turbulent wall bounded shear flows to enable prediction of the measured turbulence quantities. Perry & Chong (1982) have proposed a model which advances Townsend's (1951) ideas of attached eddies. They have associated these eddies with the presence of a hierarchy of hairpins of different sizes. The hairpins emanate from the wall and reach across varying fractions of the layer, thus, the number of hairpins influencing the flow decreases as the distance from the wall increases. Among the consequences of this model are a logarithmic region in the mean velocity profile (the consequence was first shown by Black 1968). However, it also predicts a Reynolds number independence of the turbulence intensities in the inner region, when scaled on wall variables. Experiments of Murlis *et al.* (1982) and Klewicki & Falco (1990, 1991) in boundary layers, and Wei & Willmarth (1989) in channel flows, have shown that the turbulence intensities and Reynolds stress increase faster than the friction velocity as the Reynolds number increases. The apparent discrepancy with earlier results, which indicated that wall scaling was appropriate, has been clearly attributed to probe scale resolution effects (see, for example, Klewicki & Falco 1990).

In this paper we construct a coherent motion model of the turbulent boundary layer. We then apply the model by showing that use of the typical eddy velocity and length scales enables us to remove the Reynolds number dependence of the

PHILOSOPHICAL TRANSACTIONS OF THE ROYAL SOCIETY A MATHEMATICAL, PHYSICAL & ENGINEERING SCIENCES

turbulence intensity and Reynolds stress over a wide range of Reynolds numbers. Our attention will be focused on flat plate zero pressure gradient boundary layers.

2. Coherent motions in smooth wall turbulent boundary layers

We have found that the important coherent motions observed in turbulent boundary layers can be divided into two groups: a group whose dynamics are essentially independent of the presence of the wall, which we will call the outer region subset of the overall production module (OPM), and a group that is essentially dependent upon the high shear and impermeability characteristic of the presence of the boundary, which we will call the wall region subset of the OPM. We use the term 'module' in the sense of Morkovin (1972), who defined a 'flow module' to indicate a set of correlated flow features that operate within a flow field. In our case each flow module can be divided into a number of coherent motions. We will show that the coherent motions in the wall region associated with the bursting process appear to be initiated by the outer region coherent motions. The coherent motions that define a family (for example, the typical eddies or the pockets) comprise a repetitive set of motions that have broadly similar shapes, flow signatures, evolutions and Reynolds number dependence. The descriptions of specific families given below will further clarify this concept.

The experimental technique underlying most of our experiments involves using an oil-fog containing 0.5–5.0 μm particles as a passive contaminant and simultaneous hot-wire anemometry. The anemometers are in a laser sheet that illuminates the concentration gradients that develop in the fog. The oil-fog is generally introduced at the wall upstream of the tripping device, and for some experiments it is also introduced through a slit in the wall under the developed turbulent boundary layer. In other experiments (performed in water) a number of different colour fluorescent dyes were used to passively mark the turbulence. The techniques are described by Falco (1977, 1980*a*, *b*), Lovett (1982), Chu (1987) and Chu & Falco (1988).

(*a*) *Outer region structure*

In the outer region of the turbulent boundary layer, there appear to be two important families of motions, each with its own range of scales and mode of contribution to the turbulence production. These have been called typical eddies (TEs) and large-scale motions (LSMs) by the author (Falco 1977). A large number of investigations have been made to characterize both of these: the LSMs by Kovasznay *et al.* (1970), Blackwelder & Kovasznay (1972), Antonia (1972), Chen & Blackwelder (1978), Brown & Thomas (1977), Falco (1977), Murlis *et al.* (1982), Antonia & Fulachier (1989), Antonia *et al.* (1990), and many others; the TEs have been studied by Falco (1974, 1977), Head & Bandyopadhyay (1981), Stanislas *et al.* (1987, 1990), Hoyez-Delaliaux (1990), and others.

(i) *Typical eddies*

Typical eddies are local, compact regions of vorticity concentration that have distorted vortex ring-like configurations and behaviour. Figure 1 shows examples of TEs in turbulent boundary layers at $R_\theta = 753$ and 21 300. The view is in a streamwise laser sheet that is perpendicular to the wall. At $R_\theta = 753$ the TE is a large fraction of δ (note a hot-wire probe used to obtain simultaneous quantitative data about to enter the TE). At $R_\theta = 21\,300$ two TEs are apparent. They are a small fraction of δ (see

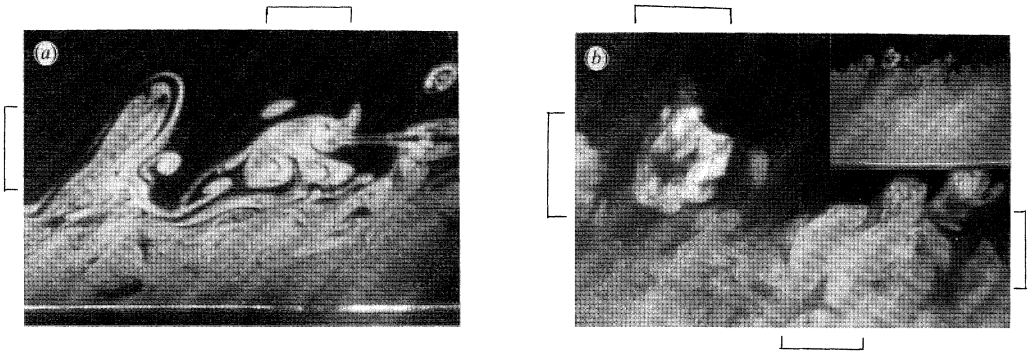

Figure 1. Photographs of TEs in turbulent boundary layers. (*a*) For $R_\theta = 753$ the TE is a large fraction of δ (note a hot-wire probe entering the TE). (*b*) At $R_\theta = 21\,300$ we see that the two TEs which are apparent are a small fraction of δ (use insert for reference). In this photo one TE has rotated so that the toroidal configuration of the ring-like TE is apparent (it has undergone the wavy core instability commonly observed in vortex rings). The photos are taken in laser sheets normal to the walls and parallel to the mean flow. Flow direction is from left to right.

Figure 2

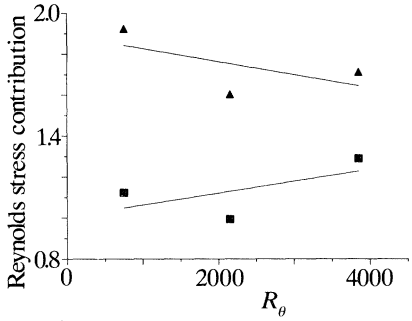

Figure 3

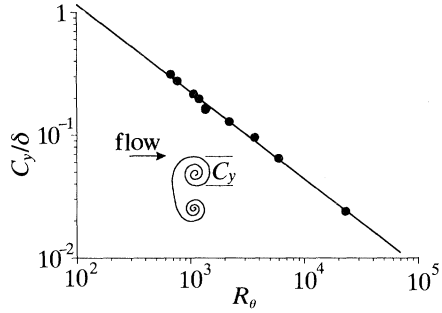

Figure 2. The ratio of ensemble averaged Reynolds stress associated with the TEs and the LSMs to the long time averaged Reynolds stress against R_θ. ▲, $\langle uv\rangle_{\text{TE}}/\overline{uv}$; ■, $\langle uv\rangle_{\text{LSM}}/\overline{uv}$. Typical eddy data were taken at $y/\delta = 0.85$, for $R_\theta = 753$; $y/\delta = 0.91$, for $R_\theta = 2157$; and $y/\delta = 0.85$, for $R_\theta = 3853$, and contain 114, 134 and 132 TEs respectively. The LSM data are for samples of 647 at $R_\theta = 753$; 557 at $R_\theta = 2157$; and 139 LSMs at $R_\theta = 3853$. Lines are least squares fits.

Figure 3. The average length scale of the visualized cores of the TEs, C_y, normalized by the boundary-layer thickness, δ, against R_θ. The curve fit is $C_y/\delta = 30.5R_\theta^{-0.758}$.

the insert showing the entire boundary layer thickness for reference). One TE has rotated so that its toroidal configuration is apparent in the laser sheet (it has undergone the wavy core instability commonly observed in vortex rings; see Maxworthy (1977) and references contained therein). The other shows a conformation remarkably similar to that of the low Reynolds number TE.

Figure 2 shows the contribution of the TEs to the Reynolds stress, obtained by conditionally sampling simultaneous visual and hot-wire data. The ratio of ensemble averaged Reynolds stress associated with the TEs to the long time averaged Reynolds stress, $\langle uv\rangle_{\text{TE}}/\overline{uv}$ as suggested by Kline & Falco (1979) has been calculated. The instantaneous Reynolds stress associated with every identifiable TE passing the hot-wire probe was sampled. Data were taken at $y/\delta = 0.85$ for $R_\theta = 753$, $y/\delta = 0.91$ for $R_\theta = 2157$, and $y/\delta = 0.85$ for $R_\theta = 3853$. Sample sizes were 114, 134 and 132

respectively. The ensemble averaged Reynolds stress contribution is significantly greater than the long time averaged Reynolds stress and appears to decrease over the measured range (the solid lines are least squares fits of the data; the large-scale motions, also shown, will be described below). Relative magnitudes such as these are representative of the fractional contributions of ensemble averaged bursts in the near wall region (see Offen & Kline 1974), and indicate that the TEs are an important contributor to the Reynolds stress in the outer part of the boundary layer. These results differ significantly from the extrapolated estimates made by Antonia *et al.* (1982). It appears that the differences are due to the fact that the basis of the extrapolation they made was not valid; it is especially dangerous to extrapolate the results of detection techniques that are looking for different events (even though, as they assumed and we will discuss below, the events do indeed have a significant degree of overlap).

Contrasted with the slow decrease in their contribution to the Reynolds stress, the length scales of the TEs decrease rapidly as Reynolds number increases. Falco (1974) estimated that $C_y/\delta = 35R_\theta^{-0.73}$, where C_y is the length scale of the diameter of the vortex core (see the definition sketch in figure 3). For the current work, a significant amount of new data has been gathered, resulting in the data and curve fit $C_y/\delta = 30.5R_\theta^{-0.758}$ shown in figure 3. This Reynolds number dependence is similar to that of the Kolmogorov microscale. However, the TE magnitude, in the range of laboratory Reynolds numbers $O(1000)$, is the order of the Taylor microscale as noted by Falco (1974), i.e. approximately 20 times the Kolmogorov microscale at $R_\theta \approx 1000$ (further comments on scaling are made below).

The measured frequency of occurrence of the TE, when normalized by the free stream velocity and boundary layer thickness, $f\delta/U_\infty$, increased from 0.78 to 1.16 as R_θ increased from 753 to 3853. This suggests that, on average, we should find about one TE per boundary layer thickness in the outer intermittent region at low Reynolds numbers (intersecting a given point), assuming the convection velocity to be close to the local mean velocity (see below).

Formation and evolution of TEs. Our overall sense obtained from several thousands of feet of visual data taken with high-speed cameras, as well as real time observations of lower speed boundary layers, and the cross-light sheet experiments of Falco (1980*a*) described above, is that the TEs have a vortex ring-like configuration and evolution, as opposed to an attached hairpin eddy configuration and evolution. At low and moderate Reynolds numbers the TEs appear to be laminar vortex rings, and thus are viscous governed. At higher Reynolds numbers the TEs have been observed to appear as wavy cored vortex rings (see figure 1*b*). At still higher Reynolds number (such as that characteristic of the atmospheric boundary layer), we have observed completely turbulent TE motions.

The formation and evolution of the TEs in a highly perturbed vortical environment strongly governs the shape of these eddies. It is unrealistic to expect that an observer will often see an idealized picture of a developing or developed TE (i.e. one appearing as an undistorted laminar or turbulent vortex ring). Since both the formation and the evolution are occurring in a fluctuating shear layer, the vortex lines are usually significantly perturbed.

Our understanding of the formation process is not yet complete, but there are indications that at least two mechanisms are involved. Formation could take place by pinch-off and reconnection of hairpins observed to lift-up from the wall (see, for example, Melander & Zabuski 1988). Falco (1983) presented data showing evolution

PHILOSOPHICAL TRANSACTIONS OF THE ROYAL SOCIETY A MATHEMATICAL, PHYSICAL & ENGINEERING SCIENCES

by this process. The experiments of Chu & Falco (1988) show the reconnection of hairpin vortices, as do the numerical simulations of Moin *et al.* (1986). The other likely mechanism is the formation of TEs from an instability of a local region of highly vortical fluid to an applied force, as described by the solutions of Cantwell (1986). These solutions describe the formation of vortex rings in an infinite fluid through the action of an impulsive force on a vortical region.

Velocity and length scales of the TEs. If we accept that the TE is a vortex ring-like coherent motion, its velocity scale is determined by its circulation and the conformation of the ring (its core radius and ring radius). This is, of course, the velocity relative to the velocity of the fluid in the boundary layer that surrounds it. By using Sallet's (1974) experimentally fitted constants in Lord Kelvin's 1867 formula, we have $U_{\text{ring}} = [\Gamma/4\pi R][\ln(8R/r) - \ln 2]$, where Γ is the circulation of the ring, R is the ring radius and r is the core radius. Sallet showed that with these constants the velocities of real rings could be closely described. R/r is typically *ca.* 3.0, where r has been defined as $\frac{1}{2}C_y$ (Falco 1977) and R is approximately $1.5C_y$. Limited data over the range of Reynolds numbers where there is visual information suggests that R/r appears to change little. Assuming it to be constant, the term in the second bracket is equal to 2.49. (The precise value of this constant will not influence the following arguments.) Thus, the velocity is approximately equal to $2.49\Gamma/6\pi C_y$. Using the definition of the circulation and Stokes' theorem, we can express the average circulation around the core of the vortex ring by $\Gamma = \boldsymbol{\omega} A = (\pi\boldsymbol{\omega} C_y^2)/4$, where $\boldsymbol{\omega}$ is the average vorticity in the TE. If the TEs are indeed the important vorticity carrying eddies in the outer region of a turbulent boundary layer, then the root mean square (rms) fluctuation of the vorticity in the outer part of the layer should be a good measure of the magnitude of their vorticity. Thus, we propose to equate the ensemble average of $\boldsymbol{\omega}$ with rms (ω'). Therefore, the characteristic velocity of the TE, u_{TE}, becomes $0.104\ \text{rms}(\omega')\, C_y$. For measurements of the eddies made in a laser sheet that is in the stream direction and normal to the wall, rms (ω_z') is the appropriate value of rms (ω'). Using these hypothesis, we can express the velocity of the TE as $u_{\text{TE}} = 0.104\ \text{rms}(\omega_z')\, C_y$.

Of particular interest is the newly discovered result (Klewicki & Falco 1990*a*) that the rms transverse vorticity, when scaled using wall variables u_τ and ν, is Reynolds number independent over the range $1000 < R_\theta < 5000$ for all values of y/δ. Wall scaling is expected because all of the vorticity is generated right at the wall in the constant density flows under consideration. A universal function can be found, which we will call $F(y^+)$. Making use of this result for the scaling of the vorticity, rms (ω_z'), we find

$$\text{rms}(\omega_z') = F(y^+)\, u_\tau^2/\nu,$$

where $F(y^+) = (0.8y^+)^{-0.5}$ for $5 < y^+ < \delta^+$. Thus, the TE Reynolds number $\Gamma/\nu = \frac{1}{4}\pi C_y^2\ \text{rms}(\omega_z')/\nu$ becomes

$$\Gamma/\nu = (\pi/4)\, F(y^+)\, C_y^2\, u_\tau^2/\nu^2 = (0.63/\sqrt{y^+})\,(Cy/\delta)^2\,(\delta u_\tau/\nu)^2$$

and the TE velocity becomes

$$u_{\text{TE}} = 0.083(y^+)^{-0.5}\, C_y\, u_\tau^2/\nu.$$

Performing an experimental correlation of available data over the range $500 < R_\theta < 60\,000$ for $u_\tau\,\delta/\nu$, we find $u_\tau\,\delta/\nu = 0.646R_\theta^{0.917}$. Combining this with the correlation of figure 3, $C_y/\delta = 30.5R_\theta^{-0.758}$, we obtain $C_y\,u_\tau/\nu = 19.7R_\theta^{0.159}$, $\Gamma/\nu = 244R_\theta^{0.318}/(y^+)^{0.5}$, and $u_{\text{TE}}/u_\tau = 1.64(y^+)^{-0.5}\,R_\theta^{0.159}$.

(ii) *LSMs*

There is general agreement about the importance of the LSM in the turbulent boundary layer. However, results from space-time correlations overstate the energy content by including the irrotational motions, and temperature and velocity discrimination techniques are generally unable to normalize the lengths (because the downstream boundaries are too poorly defined by temperature to enable discrimination) so as to enable an ensemble averaged signature to be properly constructed. Thus, we have chosen to re-examine LSMs using oil-fog smoke as the passive contaminant. The additional resource of the spatial information in each photograph enables both upstream and downstream boundaries to be identified (see figure 5). Simultaneous oil-fog laser sheet flow visualization and hot-wire anemometry using a four wire vorticity probe were used to conditionally sample the signals obtained in boundary layers. The discrimination was based on the laser sheet flow visualization. Figure 2 shows the contribution of the Reynolds stress associated with the LSMs. The ratio of ensemble averaged Reynolds stress of the LSMs to the long time averaged Reynolds stress, $\langle uv \rangle_{LSM}/\overline{uv}$, is essentially equal, but appears to show a trend to increase with Reynolds number. These data are for samples of 647 LSMs at $R_\theta = 753$, 557 at $R_\theta = 2157$, and 139 at $R_\theta = 3853$.

Figure 4 shows ensemble averaged signatures (indicated by $\langle\ \rangle$) of 557 LSMs when $R_\theta = 2157$, when the probe is at $y/\delta = 0.91$. The unsmoothed Reynolds stress, $\langle u'v' \rangle$, streamwise fluctuations, $\langle u' \rangle$, normal fluctuations $\langle v' \rangle$, $\langle \partial u'/\partial y \rangle$, $\langle \partial v'/\partial x \rangle$ and fluctuating spanwise vorticity, $\langle \omega_z' \rangle$, are shown. For each signature, the thin lines represent 1 rms about the ensemble averages (the line with the tick marks), and the dashed lines represent the zero values of the variables. The two vertical lines within the figure indicate the LSM boundaries, determined when the probe entered and left the smoke marked LSMs, which have all been normalized to the time interval between 125 and 375. There is a well-defined signature for all quantities. The Reynolds stress associated with the LSMs is confined to the upstream half of the ensemble averaged LSM (*ca.* 250–350). The ensemble averaged peak uv is twice the rms of uv. The fluctuating vorticity signature shows that vorticity is also concentrated in the upstream half. The mean vorticity is approximately $-6\ s^{-1}$, so that upstream (time greater than 375) (and downstream, time less than 125) of the LSM we are essentially in inviscid fluid. At the back (or upstream boundary, time equal to 375) of the LSM there is a strong gradient in $\langle \partial u/\partial y \rangle$, but its magnitude is very small, whereas $\langle \partial v/\partial x \rangle$ has significant magnitude. This results in high total strain-rate and low total vorticity, which is representative of a region near a convected stagnation point, rather than of a shear layer. It is interesting to note that the smoke-marked boundary quite accurately marks these gradients; if it did not they would have been significantly broadened. Examining the velocity component signatures, we see that the LSMs are primarily regions of strong velocity defect. Along with this, we see that this fluid is essentially moving away from the wall (positive values of v). In general the picture suggests that on the scale of the boundary layer, low velocity vortical fluid is moving away from the wall in the upstream half of the LSM and being turned into the main flow direction by the higher speed fluid it encounters in the outer region. Upstream of the LSM we see that high-speed fluid is moving towards the wall. Thus, the LSMs are not well characterized as rollers.

As pointed out by Falco (1974, 1977), the LSMs appear to be significantly influenced by the TEs at low Reynolds numbers. The TE scales range from $O(\delta)$ at low

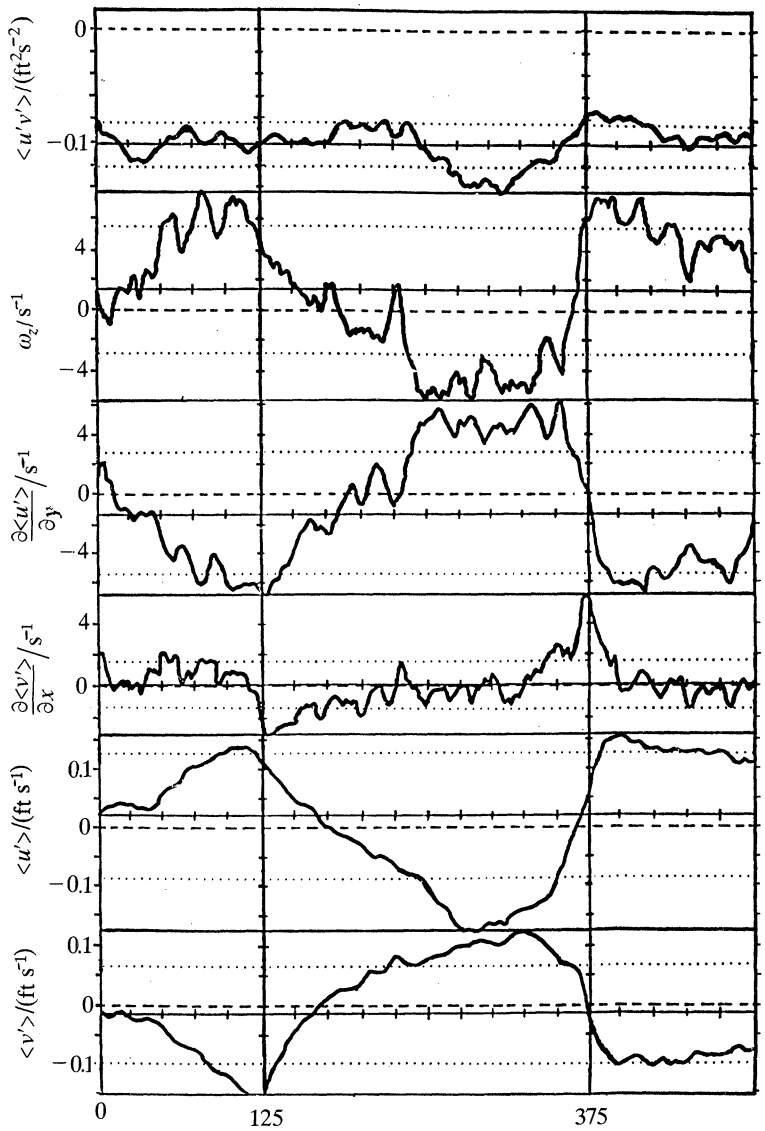

Figure 4. The ensemble averaged signals of 557 LSMs for $R_\theta = 2157$, with the probe at $y/\delta = 0.91$. The $\langle u'v' \rangle$, $\langle \omega_z \rangle$, $\langle \partial u/\partial y \rangle$, $\langle \partial v/\partial x \rangle$, $\langle u' \rangle$, and $\langle v' \rangle$ signatures are shown. Dotted lines represent 1 rms about the ensemble averages (the line with the tick marks), and the dashed lines represent the zero values of the variables. The two vertical lines within the figure indicate the normalized LSM boundaries (determined by the probe entering and exiting the smoke marked LSMs). Time increases from left to right.

Reynolds numbers to small fractions of δ as the Reynolds number increases (see figures 1 and 3). Thus, the dynamics of the LSMs are more strongly coupled to the dynamics of the TEs at low Reynolds number. As the Reynolds number increases, the influence of the TEs on the LSMs will become less than the influence of the LSMs on the TEs, as suggested by the trends in the curve fits of figure 2.

Data using two mutually orthogonal laser sheets, with one parallel to the wall and one perpendicular to the wall, allow us to see the spanwise distribution that is

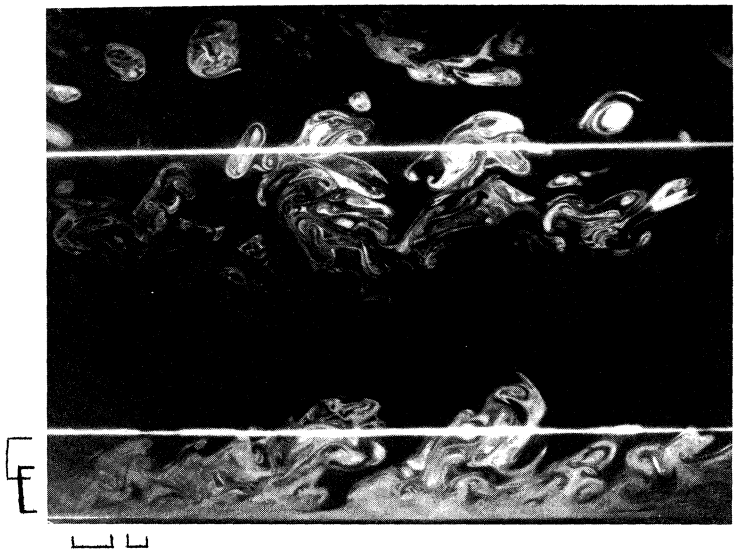

Figure 5. Simultaneous plan and streamwise views of two LSMs as seen in a split field image of two mutually perpendicular laser sheets. The plan view shows the spanwise structure of the LSMs at $y/\delta = 0.9$. The streamwise view is in a laser sheet normal to the wall and in the flow direction. Flow is from left to right. The highly irregular spanwise boundaries and deep incursions of the boundaries in the streamwise view are representative of LSM structure. Brackets indicate two TEs on the upstream boundary of the upstream LSM.

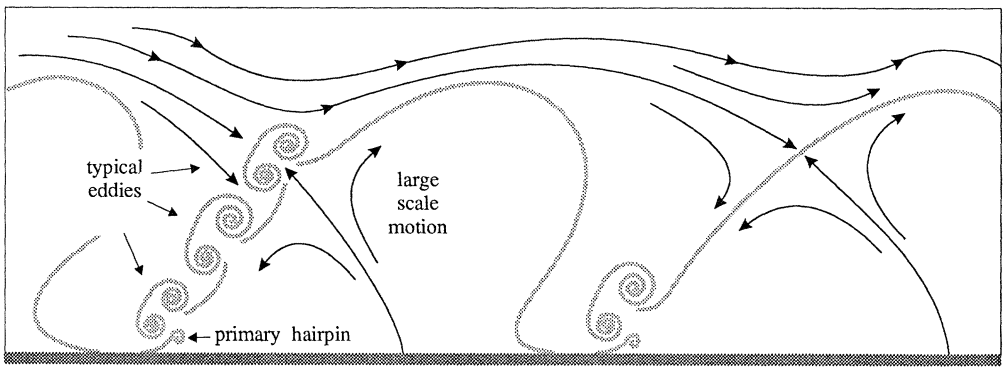

Figure 6. The outer region subset of the OPM. This includes the TEs phased to the upstream boundaries of the LSMs, and the flow of high speed fluid around and within the LSMs as seen by an observer moving with the upstream boundary of the LSMs. An indication is also given of the interaction with the wall region, which results in primary hairpin vortices (figure 8 emphasizes this interaction). The concentration gradients which distinguish the TEs, LSMs, and primary hairpins in our laser sheet flow visualizations are indicated using shaded lines.

associated with the streamwise picture. Figure 5 shows a typical result. Individual LSMs are very irregular in configuration in the spanwise direction. Thus, the ensemble averages which average the LSMs at arbitrary spanwise positions (no conditioning has been applied), are averaging over this large variation. Second, the arrangement of LSMs as seen in laser sheets parallel to the wall in the outer intermittent region, appears as a staggered array. Thus, we have a picture of regions of smoke free (potential flow or very low vorticity fluid) flowing around the LSMs in a fully three-

dimensional manner, both towards and away from the wall (see figure 6), and laterally (also see sketch in Falco 1983). The fluid that is convected will, of course, sometimes include TEs.

(iii) *Outer region subset of the overall production module*

A composite structural picture of the outer flow is presented below. It is envisioned to be a subset of the total structural picture which is responsible for the production of new turbulence in the wall region of the boundary layer. As mentioned above, this outer region composite is called the outer region subset of the OPM.

From the simultaneous flow visualization and hot-wire anemometry studies it has been found that the TEs are strongest, as well as most clearly identified, when found on the upstream side of the LSMs. This was first noticed by Falco (1977) for a low Reynolds number layer. The picture persisted in the small sample available at higher Reynolds numbers. We have now gathered evidence for this occurrence at Reynolds numbers up to 21300. Stanislas *et al.* (1989) and Hoyez-Delaliaux (1990) have studied these up to $R_\theta = 6278$, and Spina *et al.* (1991) suggest the possibility of this phasing in layers as high as $R_\theta = 80000$.

From this data base, we codify the outer region subset of the OPM. Figure 6 shows a sketch of the model. The concentration gradients which distinguish the TEs and LSMs in our laser sheet flow visualizations are indicated in the figure using shaded lines. The model consists of the TEs phased to the upstream boundaries of the LSMs, and the flow of high-speed fluid around and within the LSMs as seen by an observer moving with the upstream boundary of the LSMs. This two-family (TE and LSM), phased, coherent structure model was first presented by Falco (1977), based on visual and limited simultaneous hot-wire data. His conditionally sampled ensemble averages of the velocity field at $y^+ = 67$, showed upflow, on average, under the LSMs, and wallward flow near their upstream boundaries. When combined with the results of figure 4 (and similar x-wire results of Falco & Rashidnia (1987) for $y/\delta = 0.4$ and 0.6) the sketched flow field is suggested. We conclude that their most important property of the LSMs as far as the surrounding flow is concerned, is the magnitude of their velocity defect, which principally results in the movement of ambient high-speed freestream fluid around them, with portions moving towards the wall. The TEs are modelled as stable laminar vortex rings, with a scale dependence proportional to the Kolmogorov microscale (*ca.* $R_\theta^{-\frac{3}{4}}$). Their magnitude in the range of laboratory Reynolds numbers of $O(1000)$ as noted above is the order of the Taylor microscale. This is also between 60–$70\nu/u_\tau$ for $1000 < R_\theta < 4000$. The TEs are, on average, moving slower than the LSMs, and rapidly move outward and upstream relative to the LSM they are in. This is one important reason that they are observed to be on the upstream boundary of the LSMs: they are constantly reforming and redefining the boundaries of the LSMs in which they reside. Figures 1 and 5 (also see Falco 1977) give an indication of this phasing. Of the entire spectrum of turbulent motions, only the members of these families and their associated flow fields, are considered essential to describe the transport and entrainment that characterize the turbulence in the outer region of the boundary layer.

Transport of the TEs by an LSM is an important component of the outer region subset of the OPM. Because continuity must be satisfied, the instantaneous convected streamline pattern within and outside an LSM, as indicated in figure 6 (the lateral components of the three dimensional flow around the LSM are not shown), must be such that the TEs that are below the convected stagnation point are moved towards

the wall. The rearrangement and formation of the near-wall region motions responsible for the bulk of new turbulence are proposed to be *initiated* by the interaction of these wallward-induced TEs with the wall layer (see the OPM described below). An important feature of this interaction is that the ring-like motions are predominantly oriented such that the portion of the ring brought closest to the wall is characterized by spanwise vorticity that has a sense of rotation opposite that of the mean vorticity in the layer, Ω_z. Figure 6 also shows the onset of a primary hairpin vortex, which is the principle result of the interaction of the TE with the wall region that is apparent in these laser sheet side views.

(*b*) *Inner region*

The coherent motions of the inner region have been even more intensively studied. Our emphasis will be to integrate the various briefly reviewed features into a model of the inner region.

(i) *Streaks*

Space does not permit an extensive review of the details of the long streaky structure. Long streaks have been extensively studied (see, for example, Kline *et al.* 1967). The long streaky structure found in the wall region of turbulent boundary-layer flows is an important feature of the wall region of all bounded turbulent flows. In boundary layers the mean spacing of the overall streaky structure ($\lambda^+ = 100$) appears to be independent of Reynolds number when scaled on wall variables over the range $700 < R_\theta < 6000$ (Smith & Metzler 1983). They counted all streaks greater than 100 viscous units in length, and found that the streaks had an average persistence time in viscous units of *ca.* 500, but observed that some persisted to 2500 viscous timescales.

The mechanism of long-streak formation and the overall streak spacing is not fully understood. Early suggestions that streaks formed as a result of long streamwise vortices have not been supported by recent investigations. Head & Bandyopadhyay (1981) summarized the suggestions of many investigators that individual streaks were the result of upflow between the legs of lifted hairpin vortices. Although this is a possible mechanism, the problem is envisioning these legs, with dimensions proportional to the sublayer thickness, persisting over the timescales mentioned above. Smith (1984) suggested a model in which a long streak was the result of a series of lifting hairpins all forming in a roughly straight chain, to build up the persistence time needed to create a long streak. Falco (1980*a*) suggested that the long streaks could be formed as a result of the apparent joining of a staggered array of the streaks that bound pockets, each of which had a persistence time of the order of 30 viscous timescales (Falco 1980*c*). Chu & Falco (1988) reported that a pair of streaks will result from the passage of a TE over the wall, and performed detailed experiments showing how a vortex ring does this when interacting with a Stokes layer. The disturbance caused by a TE of scale the order of 100 viscous units readily created a streak pair of the order of a thousand viscous units as the TE moved over the wall. Falco *et al.* (1990) showed additional data and further confirmed this as a mechanism of streak formation in turbulent boundary layers. Earlier, Schraub & Kline (1965) and Oldaker & Tiederman (1977) described the formation of streaks in pairs resulting from outer region disturbances convecting over the wall. For the purposes of our coherent structure model, we will assume that streaks are the result of this inner–outer region interaction.

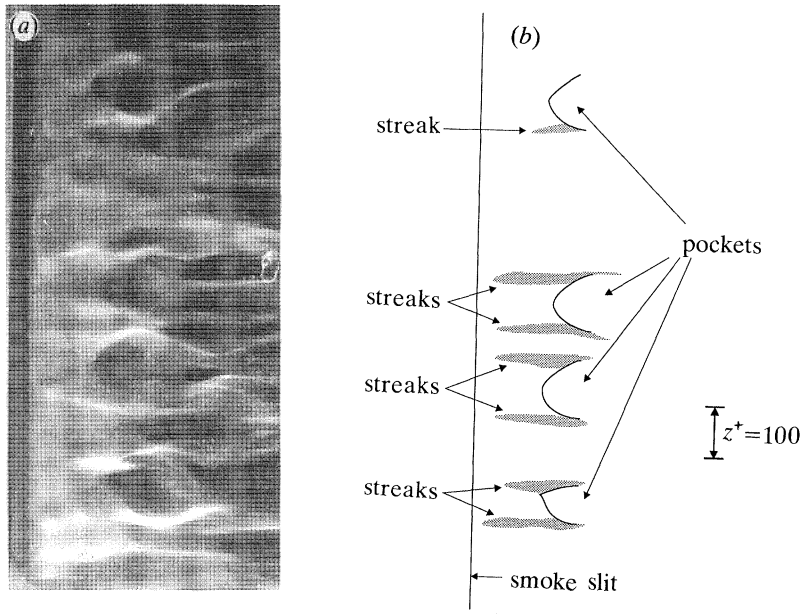

Figure 7. (*a*) Pockets forming in smoke which has emanated from a slit in the wall under a turbulent boundary layer. (*b*) indicates the position of the pockets and the downstream ends of the long streaks that are associated with them (see figure 8*c* for reference). The flow is from left to right; $R_\theta = 742$.

(ii) *Pockets*

Figure 7 shows a number of pockets which have formed in smoke emanating from a slit in the wall under a turbulent boundary layer. A pocket can form as the result of the interaction of a passing TE with the wall and the sublayer (Falco *et al.* 1990), as a result of the lift-up and formation of hairpin vortices (Smith 1988), and by the induction of outer fluid towards the wall by strong streamwise vortices (Robinson 1990). Moin *et al.* (1987) have shown that it is necessary to have sufficient concentration of marker covering an area over the wall to detect them, and that hydrogen bubble visualization does not provide enough marker, in general, to observe them. With our current understanding, it is difficult to distinguish the formation mechanism by the pocket shape alone, when viewed in plan view only. We have used a combination of filtered flood lighting and a laser sheet over the wall to determine what forms the pockets. Here emphasis is placed on pockets which are formed when an outer region disturbance causes a strong reorientation of existing sublayer vorticity. The spanwise vorticity is bunched in vortex tubes that are kinked both upstream and downstream. The region in between is a pocket. The vortex that results from the upstream bending is called the pocket vortex, and the vortex that results from the downstream bending is called the primary hairpin. As these vortices develop, the pocket continues to be defined as the region between them (see figure 8).

The pocket vortex (sketched in figure 8) becomes highly stretched (see Falco 1980*c*; Falco *et al.* 1990), because it induces itself to remain within the sublayer, where the shear is of the highest magnitude to be found within the boundary layer. Furthermore, because it is so close to the wall the impermeability condition is important, and it adds to the stretching. On the outboard sides of the pocket vortex,

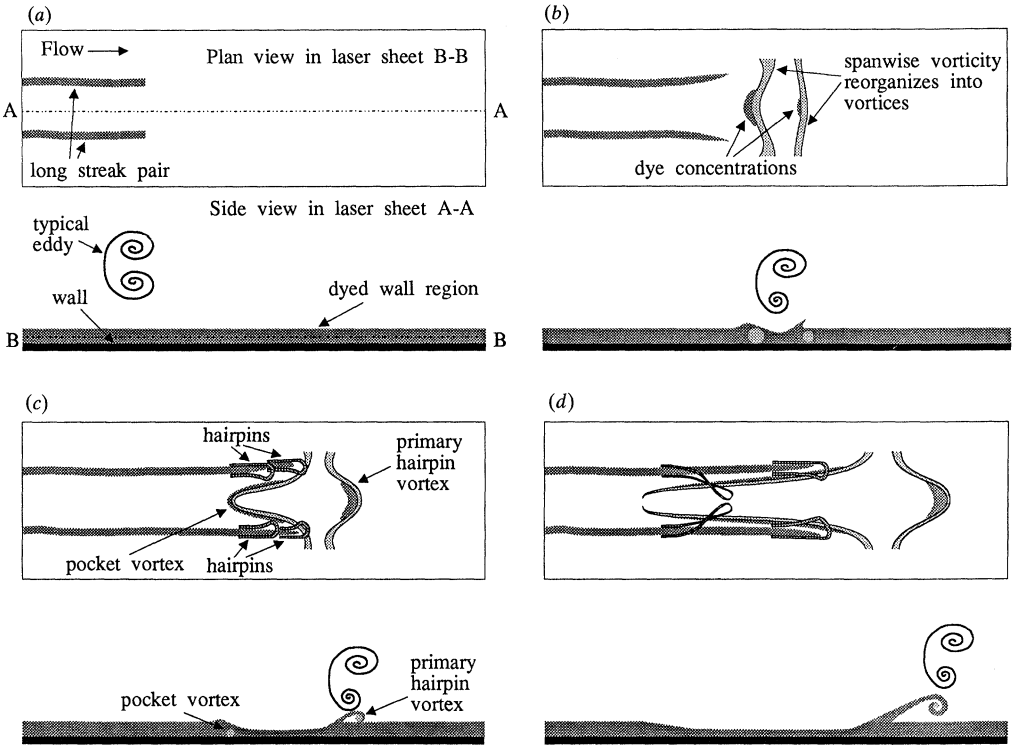

Figure 8. The OPM in plan and side laser sheet views, with the LSMs not shown (the side view of this figure essentially encompasses the region from the wall to the nearest TE in figure 6). A temporal sequence of four phases in the evolution are shown. (*a*) A TE moving over the wall rearranges dye into a pair of streaks. (*b*) The TE, having moved closer to the wall, causes a redistribution of spanwise vorticity into spanwise vortices. (*c*) Distortion of these vortices into the pocket and primary hairpin vortex; during the same time interval secondary hairpin vortices form over the streaks. (*d*) The pocket vortex is most strongly amplified by stretching, and it induces the secondary hairpins around it, moving them back towards the wall in the centre of the pocket. The primary hairpin vortex is shown lifting above the wall region. Dye concentrations (noted by darker shading) produced by the pocket vortex and primary hairpin vortex help to define the boundaries of the pocket. A symmetric picture of this process is shown for clarity, but an asymmetric picture would, in general, be expected.

where fluid is moving away from the wall, a buildup of marker occurs, forming a pair of streaks along the sides of the pocket (figure 8*c*, *d*). The mechanism for this lift-up of marker appears to be well described by Doligalski & Walker (1984). The elongation of the pocket vortex, from the moment of its formation, continually reforms the upstream and lateral boundaries of the pockets. This is clearly observed in our high-speed movies. This stretching results in very intense local vorticity. Smith *et al.* (1990) also have noted that the upstream kinks of bent vortex tubes would have the 'most active' viscous response. A further consequence of this stretching is that the pocket vortex is rapidly dissipated leaving behind a pair of streaks inside the long streak pair (see figure 8*d*).

It appears that several other investigators, including Perry *et al.* (1981) and Choi (1989), have noted the importance of pocket vortices but attributed them to upstream kinks between adjacent pairs of lifted hairpin vortices. Recently Walker

(1990) pointed out observations of an erupting ridge of contaminant of pocket shape occurs upstream of a hairpin. It is important to emphasize that pockets, as defined in the previous paragraph, have been observed to form as the result of TE–sublayer interactions. The presence of a hairpin, or pairs of hairpins, is not necessary. (I have repeatedly observed this phenomena in turbulent wall bounded flows since my first description in Falco (1978); furthermore, this can be shown to be the case in well controlled model flows, such as vortex ring–wall interactions (Chu & Falco 1988).) A feature that distinguishes the pockets resulting from outer region interactions is the presence of the hairpin vortex, which develops simultaneously with the pocket vortex and just downstream of it (refer to figure 8*b–d*). This hairpin, which we call the primary hairpin vortex, moves away from the wall, and is also stretched, but less so, because the magnitude of the strain-rate is lower than that found closer to the wall.

Falco (1980*c*) provided conditionally sampled averages of the Reynolds stress associated with the pockets and their vortices as recorded by an x-wire at $y^+ \approx 16$. The Reynolds stress associated with the pockets was comparable to that found in bursts by probe techniques such as VITA (see Blackwelder & Kaplan 1976). In the early stage of their development pockets were found to be footprints of sweeps of high-speed fluid, and during the later stages of development the pockets were characterized as marking ejections of low-speed fluid. We are using the descriptions of sweeps and ejections initiated by Corino & Brodkey (1969), in which a sweep was characterized by high-speed fluid moving towards the wall, and an ejection was characterized by low-speed fluid moving away from the wall. As the pocket evolves, the pocket vortex is stretched, frequently resulting in the lifting up of wall layer fluid and the convection of this fluid around the vortex and back down to the wall in the centre of the pocket (see figure 8*c*, *d*). As the Reynolds number increases, pockets continue to form with similar shapes (see Falco 1980*c*). However, unlike the long streaks, the spanwise scale of the pockets appears to increase when non-dimensionalized with wall variables. Figure 9 shows the average spanwise pocket scale measured at four Reynolds numbers. The scale increase is reasonably fitted by $R_\theta^{0.16}$ over the range $742 < R_\theta < 3853$, i.e. the same Reynolds number dependence that is found for the TEs (also shown in figure 9). Note that the magnitudes of the spanwise pocket scale are also approximately the same as the TE scale.

(iii) *Hairpins*

Hairpins were first suggested to be important in turbulent flows by Theodorsen (1952), and later were reported to be the 'universal element' of turbulence by Theodorsen (1955). In recent years they have been shown to be formed by at least two different mechanisms: reorganization of wall region vorticity perturbed by TEs (Falco 1982, 1983; also see Chu & Falco 1988), and by a shear layer instability of the long streaky structure (Acarlar & Smith 1987; Chu & Falco 1988). Observations of the evolution of hairpins in fully turbulent boundary layers (Falco *et al.* 1990) indicate that many of the hairpins that form from instabilities of long streaks are turned laterally and twisted back down to the wall by the pocket vortices (also see Chu 1987). Furthermore, many of the primary hairpins are ingested by TEs, and some appear to undergo reconnection resulting in new TEs (see Falco 1983). On the whole, our observations indicate that hairpins play an important role only in the near wall region. They have a short active lifetime before they transfer their momentum and are destroyed. We have observed hairpins to propagate across the boundary layers

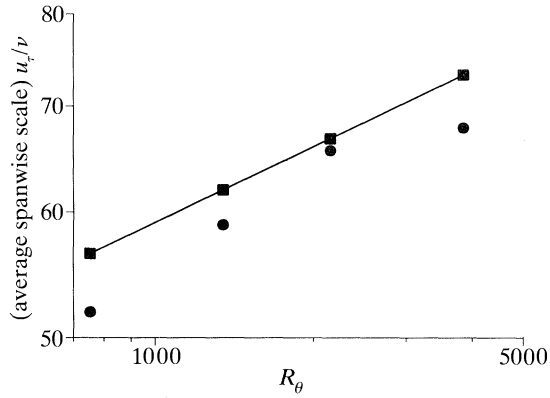

Figure 9. The TE scales, C_y ■, and the spanwise pocket scales, ●, non-dimensionalized using wall variables. Note that both the magnitude and Reynolds number dependence of the pockets are similar to those of the TE.

only in transitional flows: in the upstream region of turbulent spots, and downstream of various boundary-layer tripping devices at which the flow was separated (Falco 1982*a*).

(iv) *Wall region subset of the overall production model*

Continued observation of the coherent motions described above, primarily aided by high-speed photography, multiple light sheets, filtered flood and laser sheet combinations of illumination, and multiple dye slit injection of different colour dyes, have enabled us to find a relation between these features (see Falco 1982*b*, 1983; Chu & Falco 1988; Falco *et al.* 1990). It is necessary to have both spatial and temporal information about specifically marked regions to follow the evolution of the motions and be able to uncover the underlying relations that are responsible for the production of turbulence near a wall. Our findings led to the realization that important spatial–temporal relations exist between the coherent motions described above, which result in strong ejections of sublayer fluid as well enhanced local dissipation. We have distilled and integrated these elements into a model of the wall region flow, which we call the wall region subset of the OPM.

The plan views of figure 8 show the coherent motions that make up the wall region subset of the OPM. They initially form near the wall as a result of the perturbation by an outer region TE (shown in the side views; also see OPM discussion below). Essentially all of the contaminant redistributions and vorticity redistributions that have been observed or deduced in previous investigations are depicted in this figure. The response of the wall region provides an explanation for the existence of known wall region coherent motions, and perhaps more importantly, their interrelations and evolution. Initially the long streak pair, then the pocket and primary hairpin vortex, are formed by the TE as it gets closer to the wall (see figure 8*a*, *b*). Subsequently, the pocket and hairpin vortices evolve as indicated above, and each of the long streaks may undergo an instability that results in hairpin vortices forming along their upper boundary. Because of the spatial–temporal phasing of the long streak pair and the pocket, these hairpins initially evolve in proximity to the stretched pocket vortex. Since the pocket lies between the long streaks, these hairpins are induced to wrap around the highly stretched pocket vortex. This causes them to initially lift faster,

but then to be bent and twisted as they are moved laterally and then back towards the wall over the centre of the pocket (see figure 8*c*, *d*). This spatial coincidence between the streak related hairpins and the pocket vortex, results in an intense interaction (Falco *et al.* 1990). The fact that the TE initiates both events is essential for the pocket vortex–hairpin vortex interaction event to occur with significant frequency to be an important reason why these hairpins do not evolve into the outer region on the whole. In the physical simulations of Chu (1987), streamwise vorticity measurements using the laser induced photochemical anemometry (LIPA) non-intrusive field measurement technique (see Falco 1991), showed that the pocket vortex is 2–3 times stronger than the hairpins which form over the long streaks (in this light we see these hairpins as 'secondary' hairpins). These interactions contribute to the inward interactions (Brodkey *et al.* 1974), and each contribute about 20% of positive Reynolds stress (negative production) in the near wall region.

Thus, the wall region subset of the OPM integrates long streaks of passive contaminant, pockets, pocket vortices (with their inclined streamwise vorticity contributions), the short streaks along the sides of the pockets, and hairpin vortices of two different origins. Furthermore, the subset incorporates spatial–temporal information (as summarized in figure 8*a–d*) pertinent to the cause and effect relations between the above coherent motions.

(*c*) *The overall production module*

To better understand what initiates the streaks and pockets we must take a larger view, which encompasses the inner–outer region interaction. As indicated above, there are two important families of coherent motions in the outer region and three important scales in the inner region. The LSMs ($O(\delta)$, with a weak Reynolds number dependence), and the TEs ($O(100\nu/u_\tau)$, with a Reynolds number dependence $\sim R_\theta^{0.16}$) comprise the outer region subset of the OPM. The long-steak spacing ($O(100\nu/u_\tau)$, $500 < R_\theta < 5000$), the pockets (including both the pocket vortex and the primary hairpin vortices: lateral extent $O(100\nu/u_\tau)$ with a Reynolds number dependence $\sim R_\theta^{0.16}$), and the sublayer thickness, which is the order of the diameter of the pocket vortices ($O(5\nu/u_\tau)$) comprise the important wall region scales. The fact that both the average pocket width and the average TE scale vary as $R_\theta^{0.16}$, that the magnitude of the scales of both coherent motions are very similar, and that direct observations indicate that TEs which approach close to the wall create pockets, identify the TE as the coherent motion that links the wall region subset of the OPM and the outer region subset of the OPM. The combined modules form the OPM. Direct observations of the interactions of the two flow modules have been reported by Falco (1980*c*, 1982, 1983). More recently it has been observed that TEs can create pairs of long streaks as well as pockets (Chu & Falco 1988; Falco *et al.* 1990). Thus, the TE represents the most direct component of the coupling between the wall region and the outer region that is responsible for turbulence production. In the OPM the initiation of the wall bursting process (in the sense of Kline 1978, and Luchak & Tiederman 1987), which we identify with the wall region subset of the OPM, is phased to the upstream boundary of the LSMs, where the large-scale wallward sweeps bring the TEs towards the wall. The stronger the LSMs are, the stronger the large-scale potential flow response, and thus the larger the angle of incidence imparted to the TEs as they move over the wall. This wallward motion plays a crucial role in the inner–outer region interaction, but only in so far as these motions transport the TEs. Otherwise, the large-scale sweeps only contribute to the inactive motions (Townsend 1976), i.e. the sloshing in the wall region that is

PHILOSOPHICAL TRANSACTIONS OF THE ROYAL SOCIETY A MATHEMATICAL, PHYSICAL & ENGINEERING SCIENCES

responsible for the higher turbulence intensities in planes parallel to the wall, but not to the Reynolds stress.

A specific feature of this *initiating eddy motion* (the TE) is that it introduces positive ω_z near the wall (recall Ω_z is negative). This combines with the generally higher speed of the TE than the local speed of the wall region it has entered, to accelerate the flow beneath it, creating a sweep on the TE scale, which is embedded in the larger scale sweep that is carrying the TE. This is consistent with the observations of Grass (1971), who showed that sweeps associated with high Reynolds stress were localized in the near wall region and on average were embedded in weaker larger scale sweeps. Once excited through this perturbation, the existing near-wall region vorticity undergoes the rearrangements, and specific subsequent spatial–temporal interactions, which comprise the wall region subset of the OPM. The evolution, shown schematically in both plan and side views of figure 8, proceeds as follows. As the TE moves over the wall a distance less than its diameter away (Chu & Falco 1988), a pair of sublayer streaks forms, one on either side of the intersection of the TEs trajectory over the wall. Based upon the physical simulations of Chu & Falco (1988), this formation appears to be caused by a far-field response of the sublayer to the pressure disturbance caused by the convecting vortex ring. After (both later in time and downstream) forming the streaks on its path towards the wall, the TE comes close enough to the wall to form a pocket. This pocket forms between the streak pair, at what appears to be the downstream end of the streaks. The formation of these pockets is strongly influenced by the vorticity in the TE. The boundary-layer flow visualization (see Falco *et al.* 1990), simultaneous flow visualization and hot-wire anemometry (Lovett 1982; Falco 1978, 1982, 1983), and the physical simulations (Chu & Falco 1988) all support the point of view that this process represents the strong vortical interaction, or near field response, of the sublayer vorticity to the opposing sign vorticity in the lower portion of the vortex ring-like motion. The process has been studied in detail, in the two-dimensional case, by Doligalski & Walker (1984), who show that it leads to a strong inviscid–viscous interaction that takes the form of an eruption of the wall region flow. As the TE nears the wall its vortex ring-like character results in sublayer fluid lifting-up away from the wall on the downstream side of the TE (see figure 8), and as it does so a primary hairpin vortex is created. Experimental evidence of this process, in the form of sequences of photographs, has been shown by Falco (1978, 1982, 1983), Klewicki (1989), and, in the quasi two-dimensional case, by Doligalski *et al.* (1980). Recently, Falco *et al.* (1990) have shown that two-point vorticity–vorticity correlations statistically identify the presence of strong vortical motions consistent with the proposed picture. They placed a hot-wire probe that measures the spanwise vorticity component at $y^+ = 7.5$, 15 and 30, and traversed a second one above it. The correlation coefficient was strongly negative for the closest measured separation of $\Delta y^+ = 14.4$, reaching -0.4, and remained negative for separations at least as large as $\Delta y^+ = 120$. By definition this correlation coefficient must go to 1.0 for zero probe separation. The strong negative correlation indicates that, on average, there exists fluctuating vorticity of opposite signs at the two probes, with the spanwise vorticity at the upper probe of sign opposite that of the mean. This is consistent with the picture in figure 8, where the upper probe would be in the wallside vortex core of the TEs, and the other probe in the sublayer or buffer layer. The increasingly negative correlation as the outer probe is brought closer to the wall, indicates that the interaction between the opposing sign vortical fluctuations becomes most intense as

the outer vortical motions gets closer to the edge of the sublayer. Falco *et al.* (1990) also show that the positive ω_z motions with amplitudes greater than 1 rms have a well-defined characteristic length scale of about 25 wall units at $R_\theta = 1010$. The outer region TE scaling (determined from the smoke concentration boundaries) is 59 wall units. The data for near-wall TEs, which, because of experimental limitations, are sparser than those gathered for the outer regions, indicate that the visual scale C_y may be only 70–80 % of the outer region value for a given Reynolds number. This fact, combined with the observation of Maxworthy (1977) that rings have a very peaked vorticity distribution with long weak tails, which we would cut off in our thresholding, indicates that this scale is consistent with the expected TE scale. These findings separate the present model from others because of their ability to explain the dominant source of counter-rotating spanwise vorticity just above the wall region.

Chu & Falco (1988) have shown that the details of the TE–wall interaction depend upon a number of factors, including the instantaneous ratio of the thickness of the wall layer to the scale of the ring, the angle of incidence of the eddy with the wall, the convection velocity of the eddy, the distance of the TE from the wall layer, and the relative strengths (circulations) of both. Depending on these factors, the details of the interaction and the overall strength of the interaction will change. Thus, for example, a locally instantaneously thicker sublayer results in weaker TE–wall interactions. The angle of incidence of the ring is the second most important factor. An increase in the angle of flight with the wall results in a stronger interaction. The ratio of the convection velocity of the ring to that of the wall has a much weaker influence on the type of interaction. However, in all cases the interaction involves the creation of the pocket and the vortices described above. The length of the streak pair will depend upon the angle of incidence of the TE to the wall. Ingestion of the primary hairpin vortex, or reconnection resulting in a new TE, or movement of it back down to the wall have all been observed due to changes in the above conditions.

Therefore, we see that an important aspect of the integrated production picture (the OPM) is the discovery that strong ejections of fluid occur as a result of specific spatial–temporal relations between distinct coherent motions. The rationale for the grouping of ejections into a wall bursting process, as done by Luchik & Tiederman (1987) is consistent with our wall region subset of the OPM model. Each wall region subset is a burst, and as it passes a probe one would see a number of ejections during an average pass (see figure 8). Furthermore, because of the relation of the wall region subset of the OPM with the LSMs of the outer region subset of the OPM, we can see that quiet periods will occur between each wall region subset, which can make grouping successful. Although the wall region subset of the OPM is initiated by the TE, once initiated the evolution of the subset is governed by the dynamics of the wall region coherent motions. When we also take into account the changing influence of the LSMs on TE trajectories, and the influence of the sublayer thickness, we would not expect that either individual ejections or grouped ejections (grouped over the wall region hairpin subset) would scale on wall or outer variables. The scaling of the bursting frequency using the TE velocity is currently being explored.

3. Scaling the effects of Reynolds number

As noted in the introduction, significant Reynolds number effects have been found for both turbulent boundary layers and channels in the logarithmic region as well as further from the wall. A strong test of any coherent motion model of the boundary

PHILOSOPHICAL TRANSACTIONS OF THE ROYAL SOCIETY A MATHEMATICAL, PHYSICAL & ENGINEERING SCIENCES

layer is its ability to take into account this Reynolds number dependence. We will briefly present some of the dramatic changes that occur in the intensities and Reynolds stresses when scaled on wall variables, and show that these changes can be accounted for over most of the fully turbulent portion of the layer by the coherent structure model presented above. In particular, we will assume that the outer region ($y^+ > 30$) is dominated by only two families of motion, the TEs and the LSMs (as in the outer region subset of the OPM), and that the inner region dynamics are initiated in response to them.

(a) *Scaling using the TE length and velocity scales*

If we assume that the OPM is operative we should be able to test its ability to scale the observed Reynolds number dependence of essentially the whole range of incompressible laboratory boundary layers that have been studied. In particular, we should be able to scale the turbulence quantities rms u and $\langle u'v' \rangle$ so as to remove the Reynolds number dependence that exists when these layers are scaled using either wall variables u_τ and ν, or outer variables U_∞ and δ. Figures 10 and 11 show the results. By using the velocity of the TE, u_{TE}, as well as the length scale C_y, and the curve fit for $u_\tau \delta/\nu$ discussed above, we converted experimental data taken over a wide range of Reynolds numbers.

Figure 10*a* shows the spread in the intensity is significant in the overlap region (logarithmic region) where it had been expected, because of the existence of the law of the wall for the mean flow, that inner variables would collapse the data. A plot of these quantities in outer variables (not shown) utterly fails in the wall region. However, as figure 10*b* indicates, there is a collapse of the streamwise fluctuations throughout the wall region, the classical logarithmic region, and throughout the fully turbulent region when scaled on the TE velocity and length scales.

The peak in intensity, when plotted in wall units, now appears as a knee in the curve at approximately $y = 0.2C_y$. A universal power law relation for the intensity appears in the fully turbulent portion of the layer, the extent of which depends upon the Reynolds number. By using currently available data, the power law portion of the distribution can be fitted as

$$(\text{rms}\, u)/u_{\text{TE}} = 3.28(y/C_y)^{0.37}.$$

This relation extends for more than two orders of magnitude for the $R_\theta = 39000$ layer. The departure in the outer region is indicating the influence of both the irrotational flow in the outer region and the influence of the LSMs.

It is expected that these universal constants will see correction as more is learned about the quality of the database available, but the changes should be small. The collapse of the near wall region data indicates that the influence of the TE extends into this region, and has at least as much importance as the friction velocity and viscous length scale as close as a few viscous units from the wall (in the immediate neighbourhood of the wall viscous scales must dominate). Alternatively, the success in the wall region can be interpreted as an indication that the friction velocity associated with the turbulent boundary layer is essentially a result of the TE–wall interactions.

Figure 11*a* shows that the Reynolds stress exhibits a significantly larger variation with Reynolds number in the overlap region than the streamwise intensity when normalized using wall variables (the available data cover only a third of the Reynolds number range used in figure 10*a*). Figure 11*b* indicates the improvement in scaling the Reynolds stress when the TE length and velocity scales are used. Once

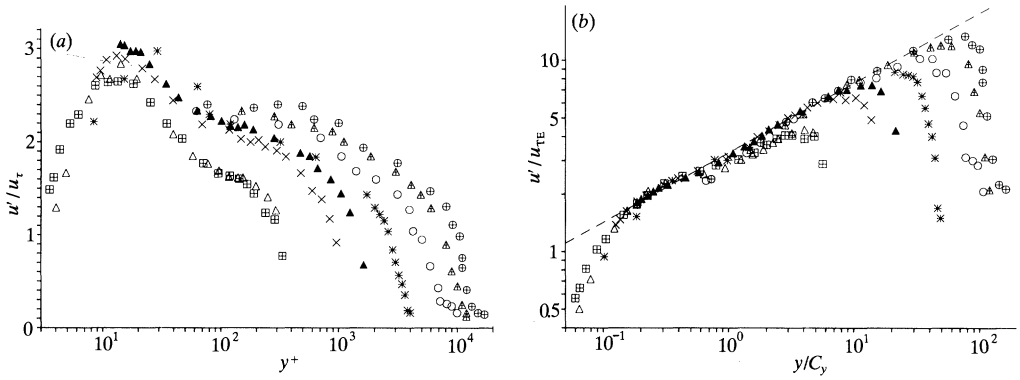

Figure 10. (*a*) The rms streamwise fluctuation (u') distributions over a wide range of Reynolds numbers, normalized using u_τ and ν/u_τ. ⊞, ×, ▲, $R_\theta = 1010$, 2870 and 4850 (Klewicki & Falco 1990); △, $R_\theta = 1340$ (Purtell *et al.* 1981); ✱, $R_\theta = 8000$ (Klebanoff 1955); ○, ⏃, ⊕, $R_\theta = 18\,300$, 28 600 and 39 000 (Petrie *et al.* 1990). (*b*) The rms streamwise fluctuation (u') distributions over a wide range of Reynolds numbers, normalized using u_{TE}, and C_y. Symbols are the same as in figure 10*a*.

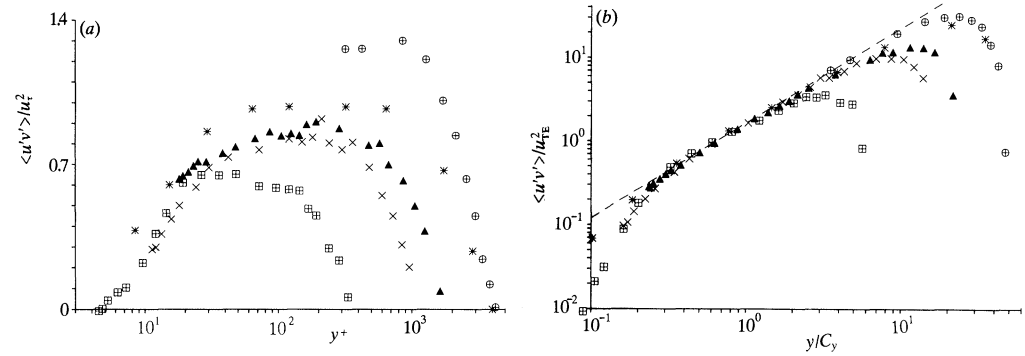

Figure 11. (*a*) The Reynolds stress $\langle u'v'\rangle$ distribution over a factor of 15 in Reynolds number, normalized using u_τ^2, ν/u_τ. ⊞, ×, ▲, $R_\theta = 1010$, 2870 and 4850 (Klewicki & Falco 1990); ∗, $R_\theta = 8000$ (Klebanoff 1955); ⊕, $R_\theta = 14\,500$ (Bradshaw & Morrison 1986). (*b*) The Reynolds stress $\langle u'v'\rangle$ distribution over a factor of 15 in Reynolds number, normalized using u_{TE}^2, and C_y. Symbols are the same as in figure 11*a*.

again we see that the overlap region (as defined by the law of the wall for the mean flow) is much better accounted for by these length and velocity scales. In addition, the fully turbulent portion of the boundary layer is also very well accounted for. A universal power law relation also exists for the Reynolds stress, over approximately the same range as found for rms u. The power law region is fitted by

$$\langle u'v'\rangle/u_{TE}^2 = 1.69(y/C_y)^{1.13}.$$

The collapse in the near wall region, with about the same accuracy as achieved using wall variables, is again suggesting that the TE influence is as important as the wall scales to within a few viscous units from the wall. The fact that both the rms u and $\langle u'v'\rangle$ distributions, which are significantly different in form (when normalized by the classical wall coordinates), can be collapsed by the TE scales from the wall region through the fully turbulent region (where the wall scaling fails) suggests the importance of the TE to boundary-layer dynamics.

4. Additional discussion

The model presented addresses the three points made by Kline & Robinson (1990) that are currently lacking consensus, and provides a framework for discussion of these issues. The points are: spatial relations among the forms of structure; temporal relations in creation, evolution and decay of structures; and a complete model of the important structure(s).

Elements of the completion of a cycle of events are inherent in the OPM. The cycle is somewhat clouded by our lack of understanding of the details of a number of possible TE formation mechanisms. Furthermore, the TEs come into the wall region to initiate the bursting process as a result of the effects of the outer region flow around the LSMs. However, the basis for regeneration is simply that highly vortical fluid reforms into TEs and is convected close enough to the wall.

The OPM suggests that the TE is an important part of the dynamics of the turbulent boundary layer at all Reynolds numbers, through its role of initiating the bursting process in the wall region. At low and moderate Reynolds numbers the TE also directly contributes to a large fraction of the Reynolds stress. However, it appears that at higher Reynolds numbers the importance of the direct contribution will diminish. It would be instructive to determine the R_θ dependence of the TE contribution, as well as that of the LSM contribution. Furthermore, detailed measurements of the TE structure are needed at high Reynolds number to determine the Reynolds number range over which the use of laminar vortex ring ideas are valid. (Evidence indicates that at high Reynolds numbers the TEs have a turbulent vortex ring character.) Furthermore, it would be of interest to determine the effect of roughness and pressure gradients on the details of the model.

There is evidence that pockets are also regions of locally high and low wall pressure. Chu (1987) studied the scale and frequency of occurrence of depressions and bulges made in a compliant surface by a turbulent boundary layer before waves set in. He found that these had both pocket length scales and frequencies. The shape, scale and evolution of the pressure patterns of Emmerling (1973) are also consistent with the pocket properties.

Our findings that pockets and TEs are Reynolds number dependent can be resolved with the data that show the overall average streak spacing is not. Since a TE produces both a pair of long streaks and a pocket, which is associated with its own streak pair, it follows that both the pocket's streak pair and the long-streak pair will also be Reynolds number dependent. However, since the streak counting procedure will include the streaks along the sides of the stretched pockets (Smith & Metzler (1983) used all streaks longer than 100 viscous units), the average streak spacing can remain independent of Reynolds number if the length of the streaks associated with pockets increases with respect to that of the long streaks as the Reynolds number increases.

This model suggests that the dissipation mechanisms of the turbulence producing motions include that of the 'attached' eddies suggested by Townsend (1951, 1976), but that other mechanisms are also important. Townsend argued that the wallward sides of streamwise oriented eddies must be close to the wall, where a dissipation layer occurs just above the viscous sublayer. The present model indicates that dissipation of the Reynolds stress carrying motions also results from their breakup when (*a*) lifted hairpins are twisted and returned to the wall by the amplified pocket vortex, and (*b*) when the primary hairpins are ingested into passing TEs and both the hairpin and TE break up. The dissipation of the pocket vortex itself, as it is

stretched, would appear to be occurring by the mechanism which Townsend suggested.

The overlap region for the Reynolds stress (defined in figure 11), where statistical quantities governed by the wall region subset of the OPM and the outer region subset of the OPM merge, can be rewritten as

$$-\overline{uv}/u_\tau^2 = 5.2R_*^{0.151}(y^+)^{0.13},$$

where $R_* = u_\tau \delta/\nu$, which explicitly shows its Reynolds number dependence in magnitude. In the classical two layer matching $\overline{uv}/u_\tau^2 = \text{const.}$ in the overlap region. Thus, this region is directly influenced by viscous as well as inertial forces. Long & Chen (1981) and Sreenivasan (1988) have previously demonstrated a Reynolds number dependence of the position of the peak values of $\overline{uv}/u_\tau^2$. However, it was tacitly assumed that the strength of the Reynolds stress remained Reynolds number independent. The data (figure 11*a*) clearly shows a dependence. The implication that viscosity plays an important role in the overlap region can be seen, in terms of our OPM, as a consequence of the importance of the process of vortex reconnection in the overlap region. As mentioned above it has been observed that the lifted primary hairpin and the TE interact, leading to breakup and reconnection (the reconnection is one of the important mechanisms in the creation of new TEs). Since vortex reconnection is the canonical example of a mechanism where viscosity is of primary importance in regions away from walls, we have identified a mechanism that could be the cause of this viscosity dependence away from the wall. It should be noted that Reynolds stress peaks have been estimated from pipe flow experiments to be as high as $y^+ \approx 500$ (Sreenivasan 1987). This emphasizes the remoteness of direct wall influence. This helps to explain why the peak Reynolds stresses can be greater than u_τ^2 even in a constant pressure boundary layer. The knee in figure 11*b* shows that there is a decided change in the Reynolds number dependence, and hence the influence of viscosity as we move away from the wall. This knee, which represents the lower bound of the overlap region, has the same R_* dependence as exhibited by the TE in viscous units. The upper bound of the interaction region is characterized by the position of the peak value of the Reynolds stress, and is proportional to $R_*^{0.5}$ (Sreenivasan 1987). Thus, both the extent and the lower bound of the overlap region move away from the wall as Reynolds number increases.

The model can be used to predict the intensity and Reynolds stress across the fully turbulent portion of constant property zero pressure gradient turbulent boundary layers over a wide range of Reynolds numbers.

5. Conclusions

An overall picture of the structure of the turbulent boundary layer has been formulated in terms of experimentally identified coherent motions. The results of simultaneous passive contaminant marker and hot-wire anemometry measurements have been reviewed. Evaluation of the data has resulted in the identification of a number of coherent motions that are important in the boundary layer (as evidenced by their contribution to the vorticity and Reynolds stress) and of specific relations that exist among the various coherent motions and their evolutions. A specific set of coherent motions in the turbulent boundary layer has been identified as the dynamically significant motions, i.e. those associated with the production of turbulence, and the transport and entrainment associated with it. The inner and

PHILOSOPHICAL TRANSACTIONS OF THE ROYAL SOCIETY A MATHEMATICAL, PHYSICAL & ENGINEERING SCIENCES

outer regions of the layer are dominated by different coherent motions which have been codified into the wall region subset of the OPM and the outer region subset of the OPM. Together they form the OPM. Important interactions and phasing that take place between the eddies in each region are reviewed. The interaction between the inner and outer region is codified as the interaction between the wall region subset of the OPM and the outer region subset of the OPM. This results from the microscale TE of the outer region subset, which is seen as initiating the wall region subset of the OPM. All of the features found by investigators of the boundary layer are embodied in these modules.

The velocity and length scales of the TE were used to scale the turbulence Reynolds stress and intensity. It was found that normalization by the TE length and velocity scales removed the Reynolds number dependence found in the inner and fully turbulent region of the boundary layer when wall scaling was used. This scaling is approximately as good as viscous scaling in the wall region (though, obviously, not right at the wall). The quality of the fits offers strong support for the OPM and allows prediction of these quantities.

Over the years many students contributed to the accumulation of data, and its reduction that has led to this picture. In alphabetical order I especially acknowledge Alan Folz, Chuck Gendrich, Jeffery Lovett, Kue Pan, David Signor and Marwan Zabdawi. This work was supported by a series of AFOSR grants, the most recent grants being AFOSR Grant-87-0047 and AFOSR Grant-89-0130 under the supervision of Dr Jim McMichael, whose encouragement and support is gratefully acknowledged. Additional support has been provided by the NASA Langley Research Center under grant NAG-1-1106.

References

Alcarlar, M. S. & Smith, C. R. 1987 A study of hairpin vortices in a laminar boundary layer, part 2. Hairpin vortices generated by fluid injection. *J. Fluid Mech.* **175**, 43–83.

Antonia, R. A. 1972 Conditionally sampled measurements near the outer edge of a turbulent boundary layer. *J. Fluid Mech.* **56**, 1–18.

Antonia, R. A., Bisset, D. K. & Browne, L. W. B. 1990 Effect of Reynolds number on the topology of the organized motion in a turbulent boundary layer. *J. Fluid Mech.* **213**, 267–286.

Antonia, R. A. & Fulachier, L. 1989 Topology of a turbulent boundary layer with and without wall suction. *J. Fluid Mech.* **198**, 429.

Antonia, R. A., Rajagopalan, S., Subramanian, C. S. & Chambers, A. J. 1982 Reynolds-number dependence of the structure of a turbulent boundary layer. *J. Fluid Mech.* **121**, 123–140.

Black, T. J. 1968 An analytical study of the measured wall pressure field under supersonic turbulent boundary layers. *NASA Contractor Report CR 888.*

Blackwelder, R. F. & Kaplan, R. E. 1976 On the wall structure of the turbulent boundary layer. *J. Fluid Mech.* **76**, 89–112.

Blackwelder, R. F. & Kovasznay, L. S. G. 1972 Time scales and correlations in a turbulent boundary layer. *Phys. Fluids* **15**, 1545–1554.

Brodkey, R. S., Wallace, J. & Eckelmann, H. 1974 Some properties of truncated turbulence signals in bounded shear flows. *J. Fluid Mech.* **63**, 209–224.

Brown, G. L. & Thomas, A. S. W. 1977 Large structure in a turbulent boundary layer. *Phys. Fluids* **20**, S243–S252.

Cantwell, B. J. 1981 Organized motion in turbulent flow. *A. Rev. Fluid Mech.* **13**, 457–516.

Cantwell, B. J. 1986 Viscous starting jets. *J. Fluid Mech.* **173**, 159–189.

Chen, C.-H. P. & Blackwelder, R. F. 1978 Large-scale motion in a turbulent boundary layer: a study using temperature contamination. *J. Fluid Mech.* **89**, 1–91.

Choi, K.-S. 1989 Near-wall structure of a turbulent boundary layer with riblets. *J. Fluid Mech.* **208**, 417–458.

Chu, C. C. 1987 A study of turbulence production and modification in boundary layers using a new photochromic visualization technique. Ph.D. thesis, Michigan State University, U.S.A.

Chu, C. C. & Falco, R. E. 1988 Vortex ring/viscous wall layer interaction model of the turbulence production process near walls. *Exp. Fluids* **6**, 305.

Coles, D. 1956 The law of the wake in the turbulent boundary layer. *J. Fluid Mech.* **1**, 191–226.

Corino, E. R. & Brodkey, R. S. 1969 A visual investigation of the wall region in turbulent flow. *J. Fluid Mech.* **37**, 1–39.

Doligalski, T. L., Smith, C. R. & Walker, J. D. A. 1980 Production mechanism for turbulent boundary layer flows: viscous flow drag reduction. *Prog. Astronaut. Aeronaut.* **72**, 47–72.

Doligalski, T. L. & Walker, J. D. A. 1984 The boundary layer induced by a convected two-dimensional vortex. *J. Fluid Mech.* **139**, 1–28.

Emmerling, R. 1973 The instantaneous structure of the wall pressure under a turbulent boundary layer flow. *Rep. 9/1973.* Max Planck Institüt, Göttingen, Germany.

Falco, R. E. 1974 Some comments on turbulent boundary layer structure inferred from the movements of passive contaminants. *AIAA Paper* 74-99.

Falco, R. E. 1977 Coherent motions in the outer region of turbulent boundary layers. *Phys. Fluids* **20**, S124–S132.

Falco, R. E. 1978 The role of outer flow coherent motions in the production of turbulence near a wall. In *Coherent structure of turbulent boundary layers* (ed. C. R. Smith & D. E. Abbott), pp. 448–461. Lehigh: AFOSR.

Falco, R. E. 1980*a* Structural aspects of turbulence in boundary layer flows. In *Turbulence in liquids* (ed. G. K. Patterson & J. L. Zakin), pp. 1–14. University of Missouri-Rolla.

Falco, R. E. 1980*b* Combined simultaneous flow visualization/hot-wire anemometry for the study of turbulent flows. *J. Fluids Engng* **102**, 174–183.

Falco, R. E. 1980*c* The production of turbulence near a wall. *AIAA Paper* 80–1356.

Falco, R. E. 1983 New results, a review and synthesis of the mechanism of turbulence production in boundary layers and its modification. *AIAA Paper* 83–0377.

Falco, R. E. 1989 Correlation of outer and passive wall region manipulation with boundary layer coherent structure dynamics and suggestions for improved devices. *AIAA Paper* 89–1026.

Falco, R. E. 1991 Laser induced photochemical anemometry, LIPA. In *Proc. ICLEO*. Boston, Massachusetts. (In the press.)

Falco, R. E. & Rashidnia, N. 1987 What happens to the large eddies when net drag reduction is achieved by outer flow manipulators? In *Proc. Symp. on Turbulent drag reduction by passive means*, pp. 477–510. London: The Royal Aeronautical Society.

Falco, R. E. & Signor, D. B. 1982*a* Evidence for the existence of vortex rings vs. hairpin eddies in turbulent boundary layers. *Bull. Am. Phys. Soc.* II **27**, 1203.

Falco, R. E. 1982*b* A synthesis and model of wall region turbulence structure. In *The structure of turbulence, heat and mass transfer* (ed. Z. Zaric), pp. 124–135. Hemisphere Press.

Falco, R. E., Klewicki, J. C. & Pan, K. 1990 Production of turbulence in boundary layers and potential for modification of the near wall region. In *Structure of turbulence and drag reduction* (ed. A. Gyr), pp. 59–68. Springer-Verlag.

Grass, A. J. 1971 Structural features of turbulent flow over smooth and rough boundaries. *J. Fluid Mech.* **50**, 233–255.

Head, M. R. & Bandyopadhyay, P. 1981 New aspects of turbulent boundary layer structure. *J. Fluid Mech.* **107**, 297–338.

Hoyez-Delaliaux, M.-C. 1990 Etude des caracteristiques instationnaires d'une couche limite turbulente de plaque plane sans gradient de pression. These de Doctorat, L'université Des Sciences et Techniques De Lille Flandres-Artois, France.

Kim, J., Moin, P. & Moser, R. 1987 Turbulence statistics in fully developed channel flow at low Reynolds number. *J. Fluid Mech.* **177**, 133–166.

Klebanoff, P. S. 1955 Characteristics of turbulence in a boundary layer with zero pressure gradient. *NACA report 1247.*

Klewicki, J. C. 1989 On the interactions between the inner and outer region motions in turbulent boundary layers. Ph.D. Thesis, Michigan State University, U.S.A.

PHILOSOPHICAL TRANSACTIONS OF THE ROYAL SOCIETY A MATHEMATICAL, PHYSICAL & ENGINEERING SCIENCES

Klewicki, J. C. & Falco, R. E. 1990 On accurately measuring statistics associated with small scale structure in turbulent boundary layers using hot-wire probes. *J. Fluid Mech.* **219**, 119–142.

Klewicki, J. C. & Falco, R. E. 1991 Effects of Reynolds number on turbulent boundary layer statistics. *J. Fluid Mech.* (Submitted.)

Kline, S. J. 1978 The role of visualization in the study of the structure of the turbulent boundary layer. In *Coherent Structure of Turbulent Boundary Layers* (ed. C. R. Smith & D. E. Abbott), pp.1–26. Lehigh: AFOSR.

Kline, S. J. & Falco, R. E. 1979 Summary of the AFOSR/MSU research specialists workshop on coherent structure in turbulent boundary layers. *AFOSR-TR-80-0290*.

Kline, S. J. & Robinson, S. K. 1990 Turbulent boundary layer structure: progress, status and challenges. In *Structure of Turbulence and Drag Reduction* (ed. A. Gyr), pp. 3–22. Springer-Verlag.

Kline, S. J., Reynolds, W. C., Schraub, F. A. & Runstadler, P. W. 1967 The structure of turbulent boundary layers. *J. Fluid Mech.* **30**, 741–773.

Kovasznay, L. S. G., Kibens, V. & Blackwelder, R. F. 1970 Large scale motions in the intermittent region of a turbulent boundary layer. *J. Fluid Mech.* **41**, 283–325.

Laufer, J. 1975 New trends in experimental turbulence research. *A. Rev. Fluid Mech.* **7**, 307–326

Long, R. R. & Chen, T.-C. 1981 Experimental evidence for the existence of the 'mesolayer' in turbulent systems. *J. Fluid Mech.* **105**, 19–59.

Lovett, J. A. 1982 The flow fields responsible for the generation of turbulence near the wall in turbulent shear flows. M.S. Thesis, Michigan State University, U.S.A.

Lu, S. S. & Willmarth, W. W. 1973 Measurements of the structure of the Reynolds stress in a turbulent boundary layer. *J. Fluid Mech.* **60**, 481–511.

Luchak, T. S. & Tiederman, W. G. 1987 Timescale and structure of ejections and bursts in turbulent channel flows. *J. Fluid Mech.* **174**, 529–552.

Maxworthy, T. 1977 Some experimental studies of vortex rings. *J. Fluid Mech.* **81**, 465–495.

Melander, M. V. & Zabuski, N. J. 1988 Interaction and apparent reconnection of 3D vortex tubes via direct numerical simulations. *Fluid Dynamics. Res.* **3**, 247–250.

Moin, P., Leonard, A. & Kim, J. 1986 Evolution of a curved vortex filament into a vortex ring. *Phys. Fluids* **29**, 955.

Morkovin, M. V. 1972 An approach to flow engineering via functional flow modules. *Beitrage zur Stromungsmechanik, A. Walz, 65th Anniversary Volume II*, Deutsche Luft und Raumfart Forschungsbericht 73–77.

Morrison, J. F., Subramanian, C. S. & Bradshaw, P. 1991 Bursts and the law of the wall in turbulent boundary layers. *J. Fluid Mech.* (Submitted.)

Murlis, J., Tsai, H. M. & Bradshaw, P. 1982 The structure of turbulent boundary layers at low Reynolds number. *J. Fluid Mech.* **122**, 13–56.

Narasimha, R. & Kailas, S. V. 1987 Energy events in the atmospheric boundary layer. In *Perspectives in Turbulence Studies* (ed. H. U. Meier & P. Bradshaw), pp. 188–222. Springer-Verlag.

Offen, G. R. & Kline, S. J. 1974 Combined dye-streak and hydrogen-bubble visual observations of a turbulent boundary layer. *J. Fluid Mech.* **62**, 223–239.

Oldaker, D. K. & Tiederman, W. G. 1977 Spatial structure of the viscous sublayer in drag reducing channel flows. *Phys. Fluids* **20**, S133–S144.

Perry, A. E. & Chong, M. S. 1982 On the mechanism of wall turbulence. *J. Fluid Mech.* **119**, 173–217.

Perry, A. E., Lim, T. T. & Teh, E. W. 1981 A visual study of turbulent spots. *J. Fluid Mech.* **104**, 387–405.

Petrie, H. L., Fontaine, A. A., Sommer, S. T. & Brungart, T. A. 1990 Large flat plate turbulent boundary layer evaluation. *Penn State Report TM 89-207*.

Robinson, S. K. 1990 NASA Langley turbulent boundary layer workshop proceedings. *NASA Langley Research Center*.

Robinson, S. K., Kline, S. J. & Spalart, P. R. 1989 Quasi-coherent structures in the turbulent boundary layer. Part II. Verification and new information from a numerically simulated flat-plate layer. In *Near wall turbulence* (ed. S. Kline & N. Afgan). Hemisphere Press.

PHILOSOPHICAL TRANSACTIONS OF THE ROYAL SOCIETY A MATHEMATICAL, PHYSICAL & ENGINEERING SCIENCES

Sabot, J. & Comte-Bellot, G. 1976 Intermittency of coherent structures in the core region of fully developed turbulent pipe flow. *J. Fluid Mech.* **74**, 767–796.

Sallet, D. W. 1974 On the translational velocities of vortex rings. *NOL Tech. Rep. 74–209*.

Schraub, F. A. & Kline, S. J. 1965 Study of the structure of the turbulent boundary layer with and without longitudinal pressure gradients. *Report MD-12*, Thermosciences Division, Stanford University, U.S.A.

Smith, C. R. 1984 A synthesized model of the near-wall behavior in turbulent boundary layers. In *Proc. 8th Symp. on Turbulence* (ed. G. K. Patterson & J. L. Zakin). University of Missouri-Rolla.

Smith, C. R. & Metzler, S. P. 1983 The characteristics of low-speed streaks in the near-wall region of a turbulent boundary layer. *J. Fluid Mech.* **129**, 27–54.

Smith, C. R., Walker, J. D. A., Haidari, A. H. & Taylor, B. K. 1990 Hairpin vortices in turbulent boundary layers: the implications for reducing surface drag. In *Structure of turbulence and drag reduction* (ed. A. Gyr), pp. 51–58. Springer-Verlag.

Spina, E. F., Donovan, J. F. & Smits, A. J. 1991 On the structure of high-Reynolds-number supersonic turbulent boundary layers. *J. Fluid Mech.* **222**, 293–327.

Sreenivasan, K. R. 1988 A unified view of the origin and morphology of the turbulent boundary layer structure. In *Turbulence management and relaminarization* (ed. H. Leipmann & R. Narasimha), pp. 37–61. Springer-Verlag.

Stanislas, M., Vandromme, D., Hoyez, M. C., Laden, T. & Pruvost, J. 1987 Etude d'une couche limite turbulente par visualization ultra-rapide par plan laser. *ONERA IMFL Report no. 87/21*, Lille, France.

Stanislas, M. & Hoyez, M. C. 1990 Analysis of the structure of a turbulent boundary layer, with and without a LEBU using light sheet smoke visualization and hot wire measurements. In *Structure of turbulence and drag reduction* (ed. A. Gyr), pp. 507–515. Springer-Verlag.

Townsend, A. A. 1951 The structure of the turbulent boundary layer. *Proc. Camb. phil. Soc.* **47**, 375–395.

Townsend, A. A. 1976 *The structure of turbulent shear flow*, 2nd edn. Cambridge University Press.

Theodorsen, T. 1952 Mechanism of turbulence. In *Proc. 2nd Midwestern Conf. on Fluid Mechanics*. Ohio State University Press.

Theodorsen, T. 1955 The structure of turbulence. In *50 Jahre Grenzschichtforschung* (ed. H. Gortler & W. Tollmien), pp. 55–62. Friedr, Vieweg and Sohn.

Ueda, H. & Hinze, J. O. 1975 Fine-structure turbulence in the wall region of a turbulent boundary layer. *J. Fluid Mech.* **67**, 125–143.

Walker, J. D. A. 1990 Models based on dynamical features of the wall layer. *Appl. Mech. Rev.* **43**, S232–S239.

Wei, T. & Willmarth, W. W. 1989 Reynolds number effects on the structure of a turbulent channel flow. *J. Fluid Mech.* **204**, 57–95.

Willmarth, W. W. 1975 Pressure fluctuations beneath turbulent boundary layers. *A. Rev. Fluid Mech.* **7**, 13–37.

PHILOSOPHICAL TRANSACTIONS OF THE ROYAL SOCIETY A MATHEMATICAL, PHYSICAL & ENGINEERING SCIENCES

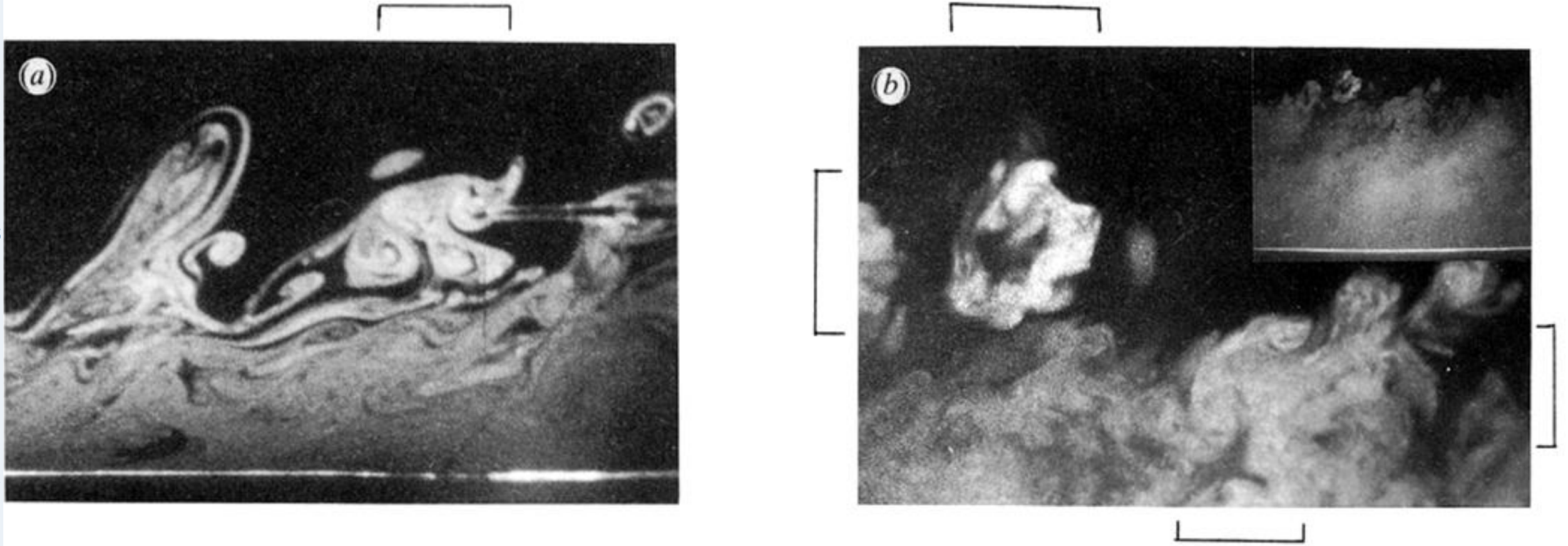

igure 1. Photographs of TEs in turbulent boundary layers. (*a*) For $R_\theta = 753$ the TE is a large action of δ (note a hot-wire probe entering the TE). (*b*) At $R_\theta = 21\,300$ we see that the two TEs hich are apparent are a small fraction of δ (use insert for reference). In this photo one TE has tated so that the toroidal configuration of the ring-like TE is apparent (it has undergone the wavy re instability commonly observed in vortex rings). The photos are taken in laser sheets normal the walls and parallel to the mean flow. Flow direction is from left to right.

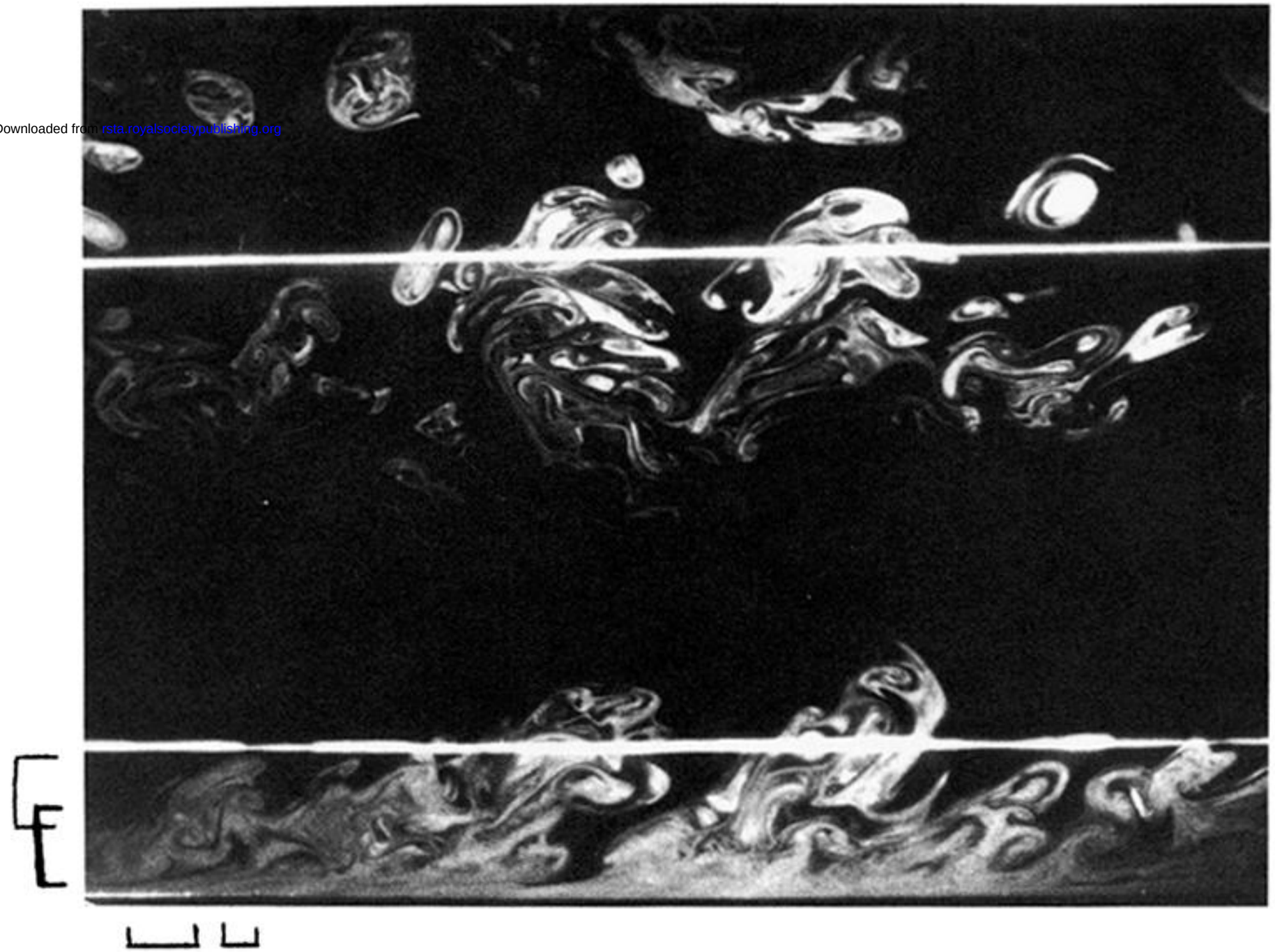

igure 5. Simultaneous plan and streamwise views of two LSMs as seen in a split field image of two utually perpendicular laser sheets. The plan view shows the spanwise structure of the LSMs at $/\delta = 0.9$. The streamwise view is in a laser sheet normal to the wall and in the flow direction. Flow from left to right. The highly irregular spanwise boundaries and deep incursions of the boundaries the streamwise view are representative of LSM structure. Brackets indicate two TEs on the ostream boundary of the upstream LSM.

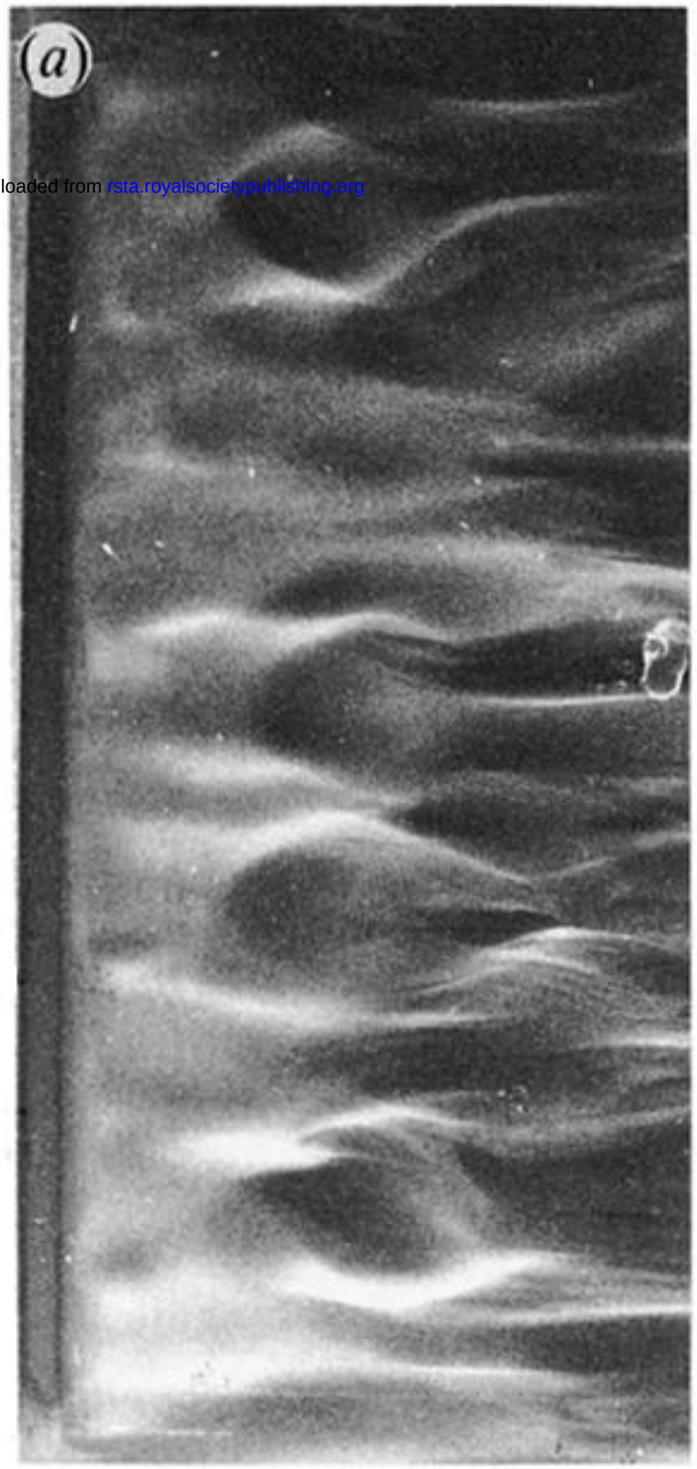

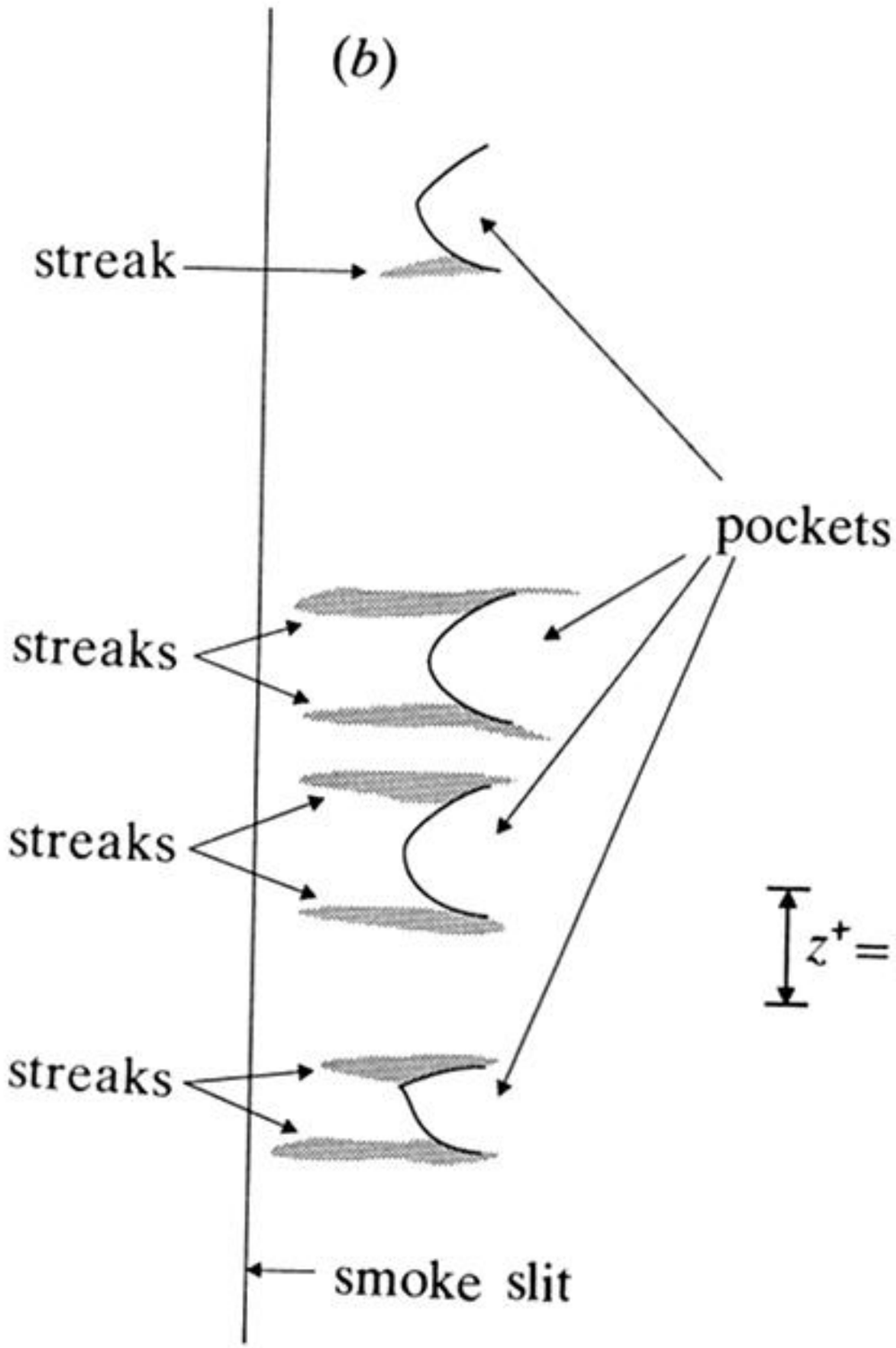

igure 7. (*a*) Pockets forming in smoke which has emanated from a slit in the wall under a urbulent boundary layer. (*b*) indicates the position of the pockets and the downstream ends of the ng streaks that are associated with them (see figure 8*c* for reference). The flow is from left to right; $_\theta = 742$.